To the editor and reviewer:

For this revision, we have addressed the new comments from Reviewers 2 and 3. Reviewer 3 found a few typos and otherwise found the manuscript to be well written and complete. We have made sure to fix the typos. Reviewer 2 had a few more questions and comments. What follows are our responses to Reviewer 2. The reviewer's comments are italicized in blue. Our responses are in black.

REVIEW: Atmospheric Blocking in an Aquaplanet and the Impact of Orography by Narinesingh et al.

Summary:
Scientific significance: good
Scientific quality: good
Presentation quality: good

I would like to thank the authors for considering my earlier comments. The manuscript is now more focused on the key questions that can be answered using the experiments and better uses previous work to explain the changes. Specially, the authors show that orography impacts the regional and hemispherically integrated statistics of blocking. The results could potentially explain differences in Northern versus Southern Hemisphere blocking and regional differences in Northern-Hemisphere blocking in reanalysis. Given the improvements, I recommend minor revisions before this paper can be published.

[Ans] Thank you for your feedback and helpful suggestions throughout the peer review process of this article. Please see below for specific responses to your comments.

General comments:

1. *Significance testing (section 2.5.4 and results): As I understand it, the authors use t-tests where the samples are taken from winter mean blocking frequencies. The t-test assumes the data are normally distributed, however, daily blocking events follow more of a Poisson distribution. Does averaging the events over one year produce normally distributed samples, either regionally or hemispherically integrated, as expected from the central limit theorem? I think it is important to confirm whether the statistical test is appropriate given that the changes in blocking statistics are modest and have large internal variability. Furthermore, have the authors tested whether the Northern versus Southern hemisphere statistics in reanalysis are statistically significant (L350-351)? Also I might be mistaken but I don't think the statistical significance mentioned on L493-494 was stated explicitly in the results section. I only found a mention of the regional blocking frequencies being significantly different on L385-390.*

   [Ans.] Thank you for pointing out the need to check the appropriateness of the t-test in our significance testing. In the figure below (Response Fig. 1), we take hemispherically averaged blocking frequency for each cool season and create histograms for each model configuration. Superimposed on these plots are the parameterized normal distributions using the mean and standard deviation.

For the 300-year aquaplanet, the histogram does indeed show behavior resembling a normal distribution in terms of shape and magnitude (response Fig. 1a). The other model configurations also show signs of convergence to a normal distribution. One caveat, however, is that the histograms for the orographic configurations (i.e. 30 years of data) appear to be under-sampled and noisy. Nevertheless, one strength of the t-test (Welch's t test in our analysis) is the test statistic is a function of both sample variances. Therefore, we deem this approach to be an appropriate method for the hemispherically averaged blocking frequency analysis.

On the other hand, if we focus on the distributions of average blocking frequency at a given gridpoint, rather than the hemispheric averages, we find that the distributions do not resemble a normal distribution. These, as you mentioned, more naturally fit Poisson distributions (not shown). Therefore, we instead use the Mann-Whitney u test for the significance testing of gridpoint-wise blocking frequency. One advantage of the u test is that it does not rely on parameterized fitting to any specific distribution. Figures 4e-h, 5b, and 9b are updated using the u test, and yield nearly identical results to the t test used before. The duration analysis also now uses as u test, which yields the same significance testing results as before. The methods section lines 250-265 are now updated to explain our choices in significance testing

Significance testing on hemispherically averaged cool season blocking frequency for the northern and southern hemispheres does indeed find that the Northern Hemisphere has significantly more blocking. Lines 375-376 now mentions this result. Though the absolute difference between both hemispheres is a modest 1.1% (2.7 % for the NH minus 1.6% for the SH), in terms of relative change, this is a 68% increase. The idealized model does not show such drastic changes from configuration to configuration, but when comparing the aquaplanet to the 3 km single mountain run for example, we still find a 15 % increase in hemispherically averaged blocking frequency. The reason for this discrepancy is discussed in greater detail in our response to your Major comment #3.

With regards to the significance results mentioned in the conclusion lines 493-494, we now explicitly mention this in the results section lines 415-416, and 429. Thank you for catching that.
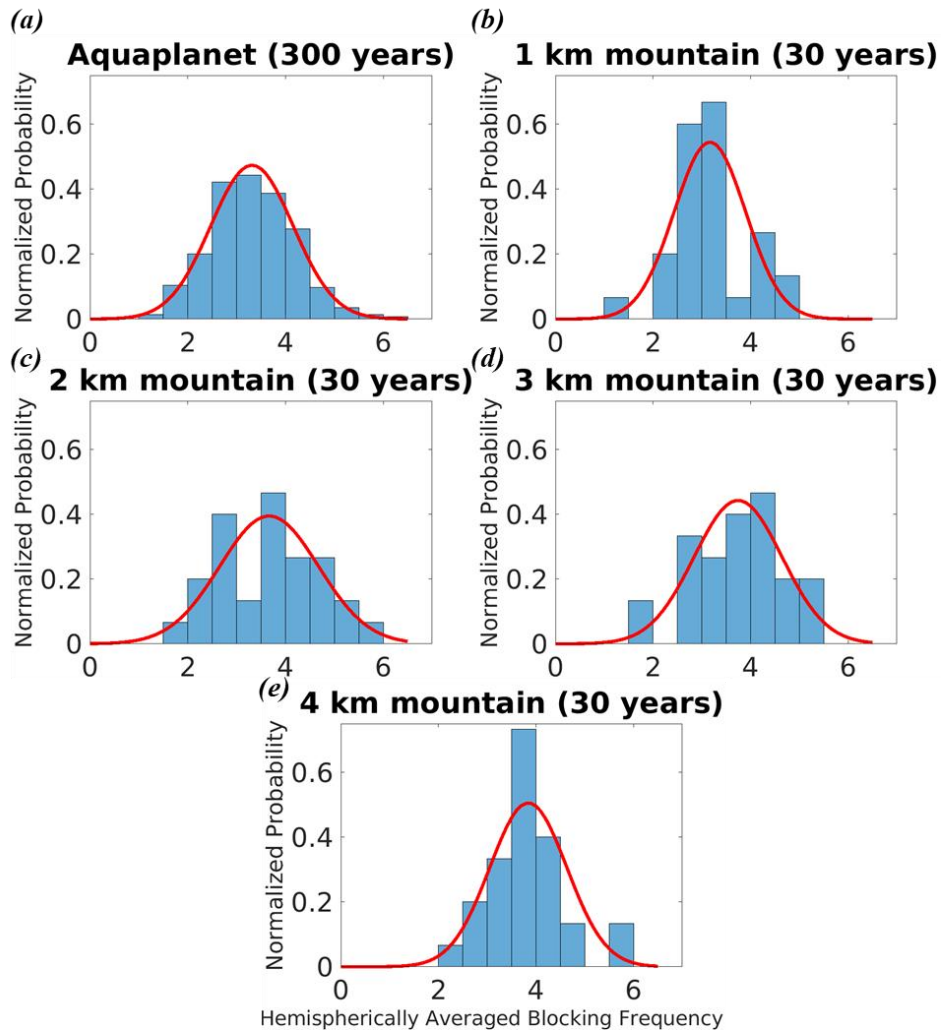
Response Figure 1. Histograms of cool season hemispheric-average blocking frequency (blue bars) and parameterized normal distributions using the sample mean and standard deviation (red curves). (a) is for the aquaplanet idealized model integration, and (b)-(e) are for the single mountain integrations of varying height.

2. *Results L279-282 and Fig. 3: I'm confused why the authors show Southern Hemisphere reanalysis results in Fig. 3a-c. I thought the idea behind the orography experiments was to mimic the configuration in the Northern-Hemisphere? I don't understand why the authors avoided 'regional variations' in Northern-Hemisphere blocking. Are the results different if Northern-Hemisphere blocks are shown? Furthermore, I'm confused why blocking events 'near the high-pressure anomaly of stationary waves' from the 3km mountain experiment was chosen. Are the results different if blocks from other regions are shown? If the authors need to be selective about which blocks to compare in the model and reanalysis, it suggests that the answer to question 1 in the Introduction is no.*

[Ans] We can see your point. We are not trying to pick and choose results, and we have adjusted the manuscript to make that point clear, as detailed below.

Figure 3 has been remade and now it includes a composite for the NH – albeit the blocks over the oceans only. As the figure shows, the block-centered composites of geopotential height anomalies, wave activity flux vectors, and wave activity flux divergence NH and SH in reanalysis and the models share many characteristics.

Our reason for not including the NH in the previous iteration of this manuscript is as follows: (1) for the sake of comparing observations with the aquaplanet, it makes sense to use the SH. , and (2) Nakamura et al., 1997, MWR, highlights the fact that the North Pacific differs from the North Atlantic in the compositing. We found the same difference they discuss: for the North Pacific the wave activity flux into the block at the initialization phase is weaker than it is for the North Atlantic. However, we agree with your point: since we are making the case that the idealized model captures many of the features found in observations, we should show it for both the NH and SH. Therefore, the text discussing the compositing has been adjusted to account for all of these changes (section 3.1). We also include a discussion of the differences between the blocks of the ocean for the North Pacific and North Atlantic. This can be found in lines 296-297, and 301-304.

Your second question is regarding why, in the 3km single mountain case, we chose to show blocks near the high-pressure anomaly of the stationary wave rather for the entire model domain (these figures are now on the bottom row of the new Figure 3). Here, we admit that up until now, we did not fully appreciate the significance of this figure – so thank you for pressing on this one.

For the previous iteration of this manuscript, we chose to show blocks in the 3km single mountain configuration from the region near the high-pressure anomaly to emphasize that they evolve in a dynamically similar manner to blocks forced without the presence of a climatological stationary wave (i.e. as in the aquaplanet). However, your questions have helped us appreciate a key difference between the model and observations: in the model configured with mountains, the regional differences in the blocking composites are smaller than those found in observations. Thus, the model is missing some aspects of the dynamics that are associated with forcing of the blocks in the NH. That being said, the model does well to capture the geographical preference for blocking to occur in regions upstream of mountains. This, we think is a useful result: despite the model with mountains not being able to fully capture the internal physics of the blocks (as revealed by the composites being so similar for the model with mountains and aquaplanet), the model configured with mountains does capture the spatial shifts in the location of the blocks. Therefore, in the conclusion we have included some commentary on this result in lines 540-549:

"We note that the influence of mountains in our model is not identical to the differences between the NH and SH in observations. First, from the block-centered composites (Fig. 3), it was clear that the NH vs SH differences in observations for Z500 anomalies and wave activity flux are larger than those found for the aquaplanet as compared to the idealized configurations with orography. This is true for the case shown in Fig. 3 (3 km single mountain) and all other model configurations with orography. Additionally, the hemispherically-averaged blocking frequency in the NH is much larger than the SH as compared to the aquaplanet versus any model configuration with mountains. On the other hand, the spatial distribution of blocking minimizes at the storm track entrance and maximizes near the anticyclonic peak of the stationary wave, is exactly captured in our model. Thus, there are some similarities for our aquaplanet and orographic configurations inconsistent with reanalysis – which may be due to deficiencies in the model (discussed below), but there are also important differences when orography is added."

3. *Discussion and conclusion section: The results show modest changes in blocking statistics when comparing individual experiments to their control simulation and some of these changes are not statistically significant. The authors chose to emphasise the differences with the control simulation rather than the similarities. While I understand the reasoning for this choice, I think the authors should also discuss the implications of the similarities, which are larger than the differences, which were mentioned in my earlier review. In particular, it could be that the model fails to capture the real effect of topography in reanalysis or that other processes, not included in the model, better explain the statistics in reanalysis.*

[Ans] We have addressed this comment by adding more commentary in the conclusion section (lines 550-563). We highlight the similarities, such as the hemispheric averages in blocking amount, but we also point out the differences in spatial distributions. We use this, plus the new composite results discussed in the response to your major comment #2 to highlight the following:

"the fact that the compositing did not show the same differences for aquaplanet vs. mountains cases as SH vs. NH implies that the subtleties of the block-centered compositing dynamics do not determine the spatial distribution of the blocks."

Specific comments:

1. *Abstract: I suggest including a sentence that states the knowledge gap in the literature to entice the reader. Its not clear why your results are important based on the abstract only.*

   [Ans] We have added to the abstract to reflect this (lines 1, and 29-31). There we mention how our results help explain some of the differences in blocking between the NH and SH as well as the importance of stationary waves. We also mention how this study shows the utility of an idealized model for understanding blocks observed in reality (lines 20-21).

2. *L72-74: Questions 1 and 4 are similar. I suggest combining them. Also I suggest changing 'overall' in question 3 with 'hemispherically integrated' to be more concise.*

   [Ans] We choose to keep questions 1 and 4 separate. Though they are linked, we find them to be distinct. Question 1 is focused on similarities in dynamical evolution of blocking between models, whereas question 4 focuses on duration. In question 2, as per your suggestion, we change "overall" to "hemispherically averaged".

3. *L260 and other subsection titles: suggest using more descriptive titles. For example: 'Lifecycle of blocking in reanalysis and the idealized model' for section 3.1.*

   [Ans] We appreciate your suggestion but it is our preference to keep the headings as is with the exception of 3.1. For this subsection, we change the name to "Blocking in the aquaplanet, dynamical aspects and intermodel comparison" to be more descriptive.

4. *L296: Needs more explanation if the Danielson et al. 2005 citation is included.*

   [Ans] We have added some context to this in lines 314-316.

5. *L307-308: Citing the Woollings paper in the Introduction would be helpful to readers.*

   [Ans] Agreed, we now add a line in the beginning paragraph of the introduction (lines 36-37):

   "For readers looking for a comprehensive review of blocking see Woollings et al. 2018."

6. *L395: For comparison, how high are the Rockies and Himalayas?*

   [Ans] We now include this in lines 421-423:

   "3 km height is meant to be semi-realistic; the values are lower than the maxima for the Rockies and the Tibetan Plateau (~4400 m and ~8800 m, respectively) – however the mountains are substantial enough to generate obvious changes in the circulation (as evidenced in the Single Mountain experiments)."

7. *418-419: Alternate explanation: other processes not included in the model could explain the differences.*

[Ans] Noted, we now include this caveat and others in the conclusion section lines 556-563.

8. *L437-439: Instead of 'cautious suggestions', a more robust statement could be made that the differences are likely due to internal variability. The non-linear changes in duration in response to linear changes in topography support this interpretation.*

[Ans] We leave the cautious suggestion part in but include your suggestion about internal variability. See lines 466-467.

9. *L459-460: I don't understand what the citation is referring to here.*

[Ans] Agreed, this was unclear. We have removed this. After some clarification, we also take out the incorrect statement that land in these experiments includes orographic drag. We now cite Pithan et al. 2016 in lines 556-558 of the conclusion instead.

10. *L475 'purely through eddy-eddy interactions': You haven't shown this. I would simply say that that blocks can be produced using a zonally symmetric model consistent with the role of eddy-eddy interaction generating blocks.*

[Ans] Thank you for the suggestion. We now adjust the wording in lines 508-509 to reflect this.

11. *Conclusions and discussion: Since the authors have laid out specific questions in the Introduction, I think it would be useful for readers if you repeated them here before answering them.*

[Ans] Agreed, we have included this reminder in the beginning of the conclusions section lines 502-507.

12. *Tables 2-3: It would help to have some measure of the year to year variability in these numbers to better understand the magnitude of the changes between experiments. For example, you could add 95% confidence intervals using +-2 standard deviations next to each value in the tables. You could also include a star symbol to denote which experiments are statistically different than the control.*

[Ans] Thank you for the suggestion. We have now included the standard deviations in this table as well as asterisks denoting statistically different results from the aquaplanet.

13. *Fig. 2 and 3: Suggest presenting both figures in the same format to better compare.*

[Ans] We choose to keep these figures as is because they provide two different, but equally useful ways of visualizing blocks. In Fig. 2 we see blocks as projected onto a sphere, whereas Fig. 3 shows blocking from an equal-area perspective.

14. *Caption in Fig. 4: I think this may be wrong.*

[Ans] Thank you for catching this error. This caption has been corrected

15. *Fig. 8: It is difficult to compare different experiments because they overlap. I suggest splitting this plot into 4 panels, each with the control and 1 experiment with the mean and the spread. Why is the two mountain experiment left out?*

This figure has been updated as per your suggestion and now includes the two mountain experiment. The two mountain experiment was originally left out to eliminate clutter, but this format is much cleaner.

Atmospheric Blocking in an Aquaplanet and the Impact of Orography

Veeshan Narinesingh[1,2], James F. Booth[1,2], Spencer K. Clark[3], Yi Ming[4]

[1]Department of Physics, City University of New York – The Graduate Center, New York, New York, 10016, United States of America

[2]Department of Earth and Atmospheric Sciences and NOAA-CESSRST, City University of New York – City College, New York, New York, 10031, United States of America

[3]Program in Atmospheric and Oceanic Sciences, Princeton University, Princeton, New Jersey, 08544, United States of America

4 Atmospheric Physics Division, NOAA Geophysical Fluid Dynamics Laboratory, Princeton, New Jersey, 08540, United States of America

Correspondence to: Veeshan Narinesingh (veenarinesingh@gmail.com)

13

Abstract.

~~This~~Many fundamental questions remain about the roles and effects of stationary forcing on atmospheric blocking. As such, this work utilizes an idealized moist GCM to investigate atmospheric blocking in terms of dynamics, ~~spatial frequency~~geographical location, and duration. The model is first configured as an aquaplanet, then orography is added in separate integrations. Block-centered composites of wave activity fluxes and height show that blocks in the aquaplanet undergo a realistic dynamical evolution when compared to reanalysis. Blocks in the aquaplanet are also found to have similar lifecycles to blocks in model integrations with orography. These results affirm the usefulness of both zonally symmetric and asymmetric idealized model configurations for studying blocking. Adding orography to the model leads to an increase in blocking. This mirrors what is observed when comparing the northern (NH) and southern hemispheres (SH) of Earth, where the NH contains more orography, and thus more blocking. As the prescribed mountain height is increased, so does the magnitude and size of climatological stationary waves, resulting in more blocking overall. Increases in blocking however, are not spatially uniform. Orography is found to induce regions of enhanced block frequency just upstream of mountains, near high pressure anomalies in the stationary waves which is poleward of climatological minima in upper level zonal wind. While block frequency minima and jet maxima occur eastward of the wave trough. This result matches what is observed near the Rocky Mountains. Finally, an analysis of block duration ~~shows~~suggests blocks generated near stationary wave maxima last slightly longer than blocks that form far from, or without orography. Overall, the results of this work help to explain some of the observed similarities and differences in blocking between the NH and SH of Earth and emphasizes the importance of general circulation features in setting where blocks most frequently occur.

1 Introduction

Atmospheric blocks are quasi-stationary anticyclones that can cause temperature extremes (Sillman et al., 2011; Pfahl and Wernli, 2012), steer hurricanes and extratropical cyclones (Mattingly et al., 2015; Booth et al. 2017, respectively), and induce persistent weather (Cassou et al., 2005; Dole et al., 2011; Brunner et al., 2018). For readers looking for a comprehensive review of blocking, see Woollings et al. 2018.

Despite the expensive and sometimes deadly impacts of blocks, many fundamental questions remain regarding their behaviour, and models tend to underpredict blocks in terms of their frequency and duration (D'andrea et al., 1998; Matsueda, 2009). As such, this paper utilizes an idealized general circulation model to expand our understanding of blocks, focusing on the representation in models configured with and without mountains.

Some have argued that blocks are consequences of an interaction between eddies and stationary waves induced by orography (Egger, 1978; Charney and Devore, 1979; Tung and Lindzen, 1979; Luo, 2005). These studies suggest mountains are critical for the overall existence of blocking and setting the location of climatological block frequency maxima. On the other hand, Shutts (1983) used a barotropic model to show that blocking flows do not necessarily need stationary forcing and can arise purely through interactions between transient eddies. Confirming this, Hu et al. (2008), Hassanzadeh et al. (2014), and Nabizadeh et al. (2019) have more recently shown that blocks do indeed occur in idealized models in the absence of zonally asymmetric forcing.

This suggests the extratropical cyclones (i.e., synoptic-scale eddies) that occur upstream of the blocking regions may be key. Colucci (1985) and Pfahl et al. (2015) show that extratropical cyclones can impact blocks downstream of the storm track exit region. In a related theory, blocks are linked to Rossby wave-breaking (Pelly and Hoskins, 2003; Berrisford et al., 2007; Masato et al., 2012), which primarily occurs in regions of weak westerly flow.

Hu. et al. (2008) presents case studies that show blocks in an aquaplanet model behave in a realistic manner. They also find that blocks in their aquaplanet model occur more frequently than what is observed in nature – regardless of hemisphere, which is contradictory to the idea that stationary waves facilitate blocking episodes. The results of Hu et al. (2008) however, are complicated by known discrepancies within the community regarding the identification (e.g. Barnes et al., 2012) and seasonality (Barriopedro et al., 2010) of blocking. In Hu et al. (2008), results from their perpetual equinox aquaplanet are compared to Weidenmann et al. (2002), who use a different block identification algorithm on reanalysis over all seasons. Thus, questions remain regarding the relative frequency of blocks with and without the presence of mountains.

The climatological spatial distribution of blocks is well documented. In the cool months of the Northern Hemisphere (NH), two main regions of blocking occur at the north-eastern edges of the Atlantic and Pacific Ocean basins (Barriopedro et al., 2006; Croci-Maspoli et al., 2007; Dunn-Sigouin et al., 2013). In the Southern Hemisphere (SH), one main region of blocking exists, located southwest of South America (Renwick, 2005; Parsons et al., 2016; Brunner and Steiner, 2017). Overall, blocking occurs more frequently in the northern hemisphere than the southern. This difference in blocking frequency is assumed to related to the stronger stationary wave in the NH (Nakamura and Huang, 2018), often attributed to more prominent

midlatitude topography and land-sea contrasts, e.g., Held et al. (2002). However, to our knowledge, no study has confirmed this assumption.

Previous work suggests that the spatial distribution of blocking frequency (hereafter, the blocking climatology) is dependent on the behaviour of the stationary waves, jet streams, and storm tracks. Nakamura and Huang (2018) for example, propose that blocking is most ubiquitous in regions where the positive anomaly in the stationary wave maximizes, and mean westerly flow is weak. Work by others on the effects of transient eddy forcing on blocks (Shutts, 1983; Nakamura et al., 1997; Takaya and Nakamura, 2001; Wang and Kuang, 2019), shows the importance of the storm tracks. The work presented here aims to better characterize the manner in which the spatial distribution of the stationary waves, jet streams, and storm tracks are linked to the blocking climatology.

This article focuses on 4 main research questions:

1. Are blocks in an aquaplanet dynamically similar to blocks in orographically forced simulations and reanalysis?
2. Does the presence of orography affect the ~~overall~~hemispherically-averaged frequency of blocking?
3. How does orography affect the spatial distribution of blocking frequency?
4. Does orography affect the duration of blocking events?

To address question 1, we use compositing analysis to compare the life cycles of blocks for an aquaplanet, reanalysis and a model with orography. For questions 2 and 3, we compare the climatology of blocking, stationary waves, jet streams, and storm tracks for models with different orographic configurations. To answer question 4, we carry out an analysis that examines the sensitivity of block duration to mountains.

2 Methods

2.1 Reanalysis data

Although the focus of this paper is on idealized numerical modelling experiments, we also present results using reanalysis to motivate our work. The reanalysis used is the ECMWF ERA-Interim dataset (Dee et al., 2011). ERA-Interim (ERAI) has been shown to represent winter midlatitude storms as well as, and in some cases better than, other reanalyses (Hodges et al., 2011). Therefore, it likely does a reasonable job at capturing atmospheric blocking. ERA-Interim is produced using a model with roughly 0.67-degree resolution, but it is available to download at different resolutions. Herein, we used data with a 1.5 x 1.5 degree horizontal resolution. For this analysis we focus only on the cool season from 1979-2017, which is defined as Nov. – Mar., and May – Sept. for the Northern and Southern Hemispheres, respectively. Blocks are most abundant during these months (Tibaldi et al., 1994; Barriopedro et al., 2010).

2.2 Idealized model configuration

This work utilizes an idealized moist GCM described by Clark et al. (2018; 2019), which is modified from that introduced by Frierson et. al. (2006; 2007) and later altered by Frierson (2007) and O'Gorman and Schneider (2008). The

model is configured to use 30 unevenly spaced vertical sigma coordinate levels, and T42 spectral resolution, corresponding to 64 latitude by 128 longitude grid points when transformed to a latitude-longitude grid. Earth-like orbital parameters are used to simulate a full seasonal cycle in solar insolation. The model includes full radiative transfer and simplified physics parameterizations of convection (Frierson, 2007), boundary layer turbulence (Troen and Mahrt, 1986), and surface fluxes. There is no treatment of cloud radiative effects or condensed water in the atmosphere.

An aquaplanet configuration is run as the control integration. For the integrations with mountains, configurations of topographical forcing are simulated by modifying the model surface height and using a simplified treatment of land following Geen et al. (2017) and Vallis et al. (2018). Like Cook and Held (1992), and following Lutsko and Held (2016), perturbations to the surface height are introduced in the form of Gaussian mountains centered at 45° N with half-widths of 15 degrees in both the latitude and longitude dimensions. Several configurations are examined in this work:

a) Aquaplanet: idealized model with no orography

b) SingleMtn: 4 separate integrations with a single Gaussian mountain centered at 45° N, 90° E of variable peak height (1 km, 2 km, 3 km, 4 km respectively)

c) TwoMtn: 1 integration with two Asymmetrically placed 3 km high Gaussian mountains centered at 45° N, 90° E and 45° N, 150° W respectively. This placement is to loosely mimic the wide (Pacific) and short (Atlantic) zonal extents of the NH ocean basins.

The 3 km SingleMtn and TwoMtn configurations are shown in Figure 1. Ocean grid cells are represented using a slab ocean with a depth of 20 m. For simplicity we prescribe uniformly zero Q-flux, meaning that we assume that in the time mean, the net flux of energy from the ocean to the atmosphere is zero at all surface grid cells. In the configurations with mountains, land grid cells are defined as locations where the height is greater than 1/100th of the maximum surface height (3 km), corresponding to a height threshold of 30 m. As in Geen et al. (2017) and Vallis et al. (2018) land is simulated by reducing the slab ocean depth to 2 m (effectively reducing the heat capacity) and limiting evaporation using a bucket hydrology model. A uniform surface albedo of 0.26 is used to obtain a global annual mean surface temperature resembling that of the Earth. Each configuration is integrated for 40 years, but the first 10 years are discarded as spin-up time. Thus, the results presented here are for years 11-40 of each integration. 6-hourly data sets are used for the analyses in this paper, and the results are presented for Northern Hemisphere cool season, defined as the 5 months centered on the minimum in solar insolation. The model data is interpolated to the 1.5 x 1.5 degree horizontal ERA-Interim resolution prior to any analysis.

2.3 Block detection and tracking

Here we use a 500 hPa geopotential height (Z500) hybrid metric that utilizes the Z500 anomaly and meridional gradient. This metric was chosen for its robustness in terms of capturing high amplitude events involving wave-breaking (Dunn-Sigouin et al., 2013), and because it only requires the Z500 field – which simplifies tracking when analyzing large datasets. Barnes et al. (2012) finds that utilizing a Z500 metric produces similar blocking durations and climatologies to both potential vorticity and potential temperature based metrics. Blocks are detected and tracked using the algorithm described by

Dunn-Sigouin et. al. (2013), hereinafter as DS13, which is an adaptation of previous methods by Barriopedro et al. (2010) and Sausen et al. (1995). This algorithm searches for large, contiguous regions of persistent, high amplitude, positive anomalies in the Z500 field. Within these regions, Z500 must satisfy a meridional gradient reversal condition. What follows is an overview of the block identification algorithm, but specific details can be found in DS13:

1. Z500 Anomaly Calculation: For each grid-point poleward of 30 N, from the raw Z500 field subtract the running annual mean and mean seasonal cycle as computed in DS13.

2. Normalize each anomaly value by the sin of its latitude divided by sin of 45 degrees, i.e. $\frac{sin(\phi_{ij})}{sin(45°)}$, where ϕ_{ij} is the latitude of an arbitrary grid-point with longitude i and latitude j. This normalized anomaly will be referred to as ~~Z500'~~ $Z500'$.

3. For each month, in a 3-month window centered on a given month, calculate the standard deviation, S, of all ~~Z500'~~ $Z500'$ values.

4. Amplitude threshold: Identify contiguous regions of positive ~~Z500'~~ $Z500'$, greater or equal to 1.5*S.

5. Size threshold: Regions must be at least 2.5 x 10^6 km^2 in area.

6. Gradient Reversal: The meridional gradient of the Z500 field within candidate regions must undergo a reversal in sign as described by DS13.

7. Quasi-stationary condition: For each timestep, regions must have a 50 % area overlap with its previous timestep (modified from DS13's 2 day overlap which was applied to daily mean data)

8. Blocks must meet the above criteria for at least 5 days (e.g. 20 6-hourly timesteps)

In case studies using ERAI and the idealized configurations described here, it was observed that two existing blocks sometimes merged with one another to form a single, larger block. We objectively identified this merging process based on extreme shifts in the location of the block centroid (defined as the gridpoint that is the centroid of the anomalous area associated with the block). If the centroid shifted by more than 1500 km from one 6-hourly snapshot to the next, we labelled the block as a merged event. These merged events represented 23-27 percent of the total initial blocks found in the idealized model integrations. We judge these events to be unique in terms of their relationship between block duration. Furthermore, the merger-blocks create uncertainty in terms of defining a block centre for the sake of our block-centered composite analysis. Therefore, we have excluded the merged events from our block-centered compositing and block duration analyses. The blocking climatological analysis on the other hand, retains all blocks since the primary focus is on the spatial distribution of block frequency, not the individual blocks themselves.

2.4 Analysis metrics

The metrics used to characterize climatological features and blocking in the idealized model data and reanalysis are outlined below.

2.4.1 Stationary Wave and Eulerian Storm Track

The cool season stationary wave at each point is defined as the anomaly with respect to the zonal mean of the cool season climatology for the 250-hPa geopotential height field: $Z^* = \overline{Z} - [\overline{Z}]$, where brackets indicate the zonal mean and overbar indicates the time mean over cool season days for all years. This is computed separately for each gridpoint.

The Eulerian storm track is presented as the standard deviation of a 24-hour difference of the daily mean Z500 field during cool season (Wallace et al., 1988; Guo et al., 2009; Booth et al., 2017). Consider $Z_{500}(t)$ to be the daily mean Z500 value for an arbitrary gridpoint. To obtain the storm track:

1. The 24-hour difference, Z_{500}^{τ}, at each gridpoint is taken as:

$$Z_{500}^{\tau} = Z_{500}(t+1) - Z_{500}(t)$$

2. Then, the standard deviation of Z_{500}^{τ} for all cool season timesteps at each gridpoint is taken to obtain the cool season Eulerian storm track value at that point.

This is computed separately for each gridpoint.

2.4.2 Blocking and Zonal Wind Climatologies

The spatial distributions of blocking frequency, referred to hereinafter as the blocking climatologies, are calculated by averaging the block identification flag (1 or 0 respectively) per gridpoint over all cool season days. Thus, the blocking climatologies show the percent of cool season timesteps a block (as defined here) is present. This is computed separately at each gridpoint.

The 250 hPa zonal wind climatology, hereinafter referred to as $\overline{U250}$, is presented as the time mean of the 250-hPa zonal wind over the cool season months at each gridpoint.

2.4.3 Wave activity flux vectors

To better characterize the dynamical evolution of blocks within each model, wave activity flux vectors (hereinafter, $\vec{W}$) are calculated as described by Takaya and Nakamura (2001), hereinafter TN01. The wave activity flux relates eddy feedback onto the mean state and is essentially the pseudo-momentum associated with Rossby waves. Convergence of $\vec{W}$ is associated with blocking and an overall slowing or reversal of westerly flow. The formulation of $\vec{W}$ in TN01, includes a stationary term that dominates for quasi-stationary, low frequency eddies (i.e. 8- to 30-day timescales), and a non-stationary, group-velocity dependent term that is more relevant for higher frequency eddies. Here we calculate only the stationary, horizontal component of $\vec{W}$, and focus on contributions solely from the low frequency eddies.

195   Block centered composites (as described in Sect. 2.5.1. of this paper) are computed using $\vec{W}$ for each block during

196 various stages of the block's lifecycle. The horizontal components of $\vec{W}$ are calculated as in TN01. For this, eddy fields are

197 computed with an 8- to 30-day bandpass filter. This is what is described as low frequency eddies in TN01 and Nakamura et

198 al. (1997). $\vec{W}$ are given by:

199

200
$$\vec{W} = \frac{p\,cos\,\phi}{2|\vec{U}|} \begin{pmatrix} U\left(v'^2 - \frac{\Phi'}{f}\frac{\partial v'}{\partial x}\right) + V\left(-u'v' + \frac{\Phi'}{f}\frac{\partial u'}{\partial x}\right) \\ \dotsi \\ U\left(-u'v' + \frac{\Phi'}{f}\frac{\partial v'}{\partial y}\right) + V(u'^2 + \frac{\Phi'}{f}\frac{\partial u'}{\partial y}) \end{pmatrix}$$

201 This calculation is performed on variables on the 250-hPa pressure surface. For each point p is the pressure and ϕ is latitude.

202 $\vec{U}$ is the 30-day low-pass filtered horizontal wind vector with zonal and meridional components U and V, respectively. The

203 anomalous zonal wind, meridional wind, and geopotential are given by u', v', and Φ', respectively. Derivatives are computed

204 using finite-differencing, where zonal derivatives are weighted by latitude. $\vec{W}$ are given in m^{2}s^{-2}.

205

206 **2.5 Analysis methods**

207 **2.5.1 Block-centered compositing**

208   The ~~Z500',~~Z500', $\vec{W}$, and $\nabla \cdot \vec{W}$ fields are composited around the centroid of each block for the first, strongest, and

209 final days of each block lifecycle. To account for the convergence of meridians, relevant fields are projected onto equal-area

210 grids before compositing. The initial time step of a block is the first timestep that the block satisfies the amplitude, size, and

211 reversal conditions. The strongest time step of a block is defined as the time step with the greatest Z500'~~Z500'~~ (at a single

212 lat/lon location) within a block. The final timestep is the last timestep a block satisfies the amplitude, size, and reversal

213 conditions.

214   The composites presented in this paper, only include midlatitude-blocks whose centroid are always south of 65˚ N.

215 This is because we find that the high-latitude blocks exhibit distinct physical ~~behaviour~~behavior. From reanalysis data, high-

216 latitude blocks in the Southern Hemisphere have different dynamical evolution and different impacts on the surrounding flow,

217 as compared to midlatitude blocks (Berrisford et al., 2007). The 65˚ N cut-off was chosen after estimates showed this to be

218 near the minimum in the meridional potential vorticity gradient, and thus the northern limit of the midlatitude waveguide (e.g.

219 Wirth et al. 2018). Compositing results were robust to changes in cut-off latitude of +/- 7.5˚.

220

221 **2.5.2 Separating blocks by region**

222   To compare the dynamical evolution of blocks originating near the eastern edge of the ocean basins (denoted as

223 "East", near the windward side of mountains and the high-pressure maxima of stationary waves) against blocks originating

224 elsewhere (denoted as "Other"), blocks are sorted by their centroid location during their first timestep. These regions are
225 outlined in Table 1 and shown in Figure 1. The East region spans 30˚-65˚ N for 90 degrees of longitude upstream and inclusive
226 of the mountain ~~centre~~center. For the TwoMtn configuration, "East" and "Other" refer to two regions within the zonally larger
227 ocean basin (which we refer to as the "Wide Basin"), whereas blocks originating within the zonally smaller ocean basin are
228 denoted as from the "Short Basin".

229

230 **2.5.3 Block duration probability density distributions**

231 Block duration is defined as the time interval from the initial identification timestep to the end of that block's existence
232 – based on the block identification algorithm (described in Sect. 2.3). Each block is thus assigned one duration value. The
233 steps taken to obtain block duration probability density distributions are as follows:

234   1. Sort blocks into subsets by model configuration and/or basin.
235   2. Allowing replacement, randomly select a set of block durations within a given subset. The size of the random set
236   is given by the number of blocks in the subset being ~~analysed~~analyzed.
237   3. Place the durations yielded by step 2 into n equal sized bins (n=8 for figures in this paper) ranging from the
238   minimum to maximum duration of cool season blocks between all model configurations.
239   4. Steps 2 and 3 are then repeated m times (m=1000 for figures in this paper) to produce an ensemble of m
240   probability density distributions for each subset.
241   5. For a given subset, the mean probability density distribution is computed by taking the mean of that subset's
242   distributions. This is then smoothed using a running mean.
243   6. For a given subset, the standard deviation of probability density distribution is computed by taking the standard
244   deviation of that subset's distributions
245 The results of this paper are nearly constant with respect to changes in the values of n (+/- 2) and m (+/- 200). For all
246 configurations, distributions and mean values presented for duration exclude any high-latitude blocking (blocks whose centroid
247 are ever poleward of 65° N). 65° N was found to be the most appropriate cut-off in each configuration for the same reasons as
248 described for the aquaplanet compositing.

249

250 **2.5.4 Statistical significance**

251 For a given gridpoint and cool season, a block frequency value is computed by averaging all the block identification
252 flag values (1 or 0) for each timestep of that cool season. This is done at every gridpoint for every cool season to yield a 3D
253 matrix of dimensions latitude by longitude by number of years. ~~2 sample t~~ Mann-Whitney u-tests are ~~then~~
254 ~~performed~~implemented for corresponding gridpoints between a given ~~topographic~~orographic configuration and a 250-year
255 aquaplanet integration. One strength of the u-test is that it does not rely on parametric fitting to any specific distribution. We
256 therefore find this test to be more appropriate than other tests such as the t-test which requires fitting to a normal distribution.
257 A 250-year aquaplanet integration is used because the blocking climatology is more zonally symmetric when compared to

258 climatology calculations that use less years. This is done to identify regions of enhanced and suppressed blocking frequency

259 in the topographic integrations.

260   Significance testing ~~in~~for hemispherically averaged block frequency statistics are done by calculating area averaged

261 blocking frequency for each cool season. For each configuration, this yields a one-dimensional array of values ~~for each cool~~

262 ~~season. A 2-sample~~with a length that matches the number of years in the simulation. A 2-sample Welch's t-test is then used to

263 examine significant differences in hemispherically averaged block frequency between idealized model configurations. We find

264 this t-test to be appropriate for this analysis because it accounts for the variances of both samples, and distributions of

265 hemispherically averaged blocking frequency were found to be normally distributed (not shown).

266   Significance testing for mean block duration also utilizes a ~~2-sample t~~u-test to compare differences between the

267 various configurations and regions. A 95% confidence interval is imposed as the significance threshold for all significance

268 testing.

269

270 **3 Results**

271 **3.1 Blocking in the aquaplanet, dynamical aspects and intermodel comparison**

272   On average, 12.9 blocks per cool season are identified for each hemisphere of the aquaplanet. The presence of

273 blocking in this model configuration is consistent with previous studies that also find blocking in GCM's with zonally

274 symmetric forcing (Hu et al., 2008; Hassanzadeh et al., 2014, Nabizadeh et al., 2019). Figure 2 shows a snapshot of the first

275 day of an arbitrary block in the aquaplanet. Upstream and coincident with the block, a Rossby wave pattern can be observed

276 in both the Z500 and Z500'~~Z500'~~ fields (Fig. 2 - the Z500 contours show a wave-like feature, and the Z500'~~Z500'~~ field shows

277 an alternating pattern of low and high anomalies in the zonal direction). The presence of these features during the formation

278 of a block agrees with previous work for both simplified (Berggren et al., 1949; Rex, 1950; Colucci, 1985; Nakamura et al.,

279 1997; Hu et al., 2008), and comprehensive models (TN01; Yamazaki and Itoh, 2013; Nakamura and Huang, 2018; Dong et

280 al., 2019).

281   In Figure 2 near 75-85° W, a characteristic overturning of the Z500 contours indicative of anticyclonic Rossby wave

282 breaking (Masato et al., 2012; Davini et al., 2012) is also observed. Concentrated, large magnitude $\vec{W}$ are found just upstream

283 of, and propagating into the block, and a relative absence of large magnitude $\vec{W}$ ~~occur~~occurs downstream of the block. On the

284 ~~upstream,~~ downstream-equatorward flank of the block, converging $\vec{W}$ consistent with a slowing of the zonal mean flow is

285 observed. The behavior of $\vec{W}$ during the genesis of this block case study agrees with Nakamura et al. (1997) and TN01 and is

286 consistent with Nakamura and Huang's (2018) description of blocking as a traffic jam of wave activity fluxes.

287   Block-centered compositing analysis is used to confirm that, on average, the blocks identified in the aquaplanet model

288 evolve in a dynamically similar manner to models with zonally asymmetric forcing. Figure 3 shows block centered composites

289 of Z500',~~Z500',~~ $\vec{W}$, and $\nabla \cdot \vec{W}$ for blocks over the NH oceans, and for the SH as well (Fig. 3 rows 1 and 2, respectively). In

290 both panels only blocks anchored in the ~~SH~~ midlatitudes are considered (i.e., occurring between 30° and 65° of latitude~~)~~)). For

291 the sake of ~~ERA Interim (ERAI SH, left column, Figs. 3a c),~~ comparison with the aquaplanet ~~midlatitudes (middle column,~~

292 ~~Figs. 3d f),,~~ blocks over land are excluded. For the idealized model, we show blocks from the aquaplanet (Fig. 3, row 3) and

293 the East region (see table 1 and ~~figure~~Fig. 1) of the 3 km single mountain configuration (3 km SingleMtn East, ~~right column,~~

294 ~~Figs. 3g i). ERAI SH~~ Fig. 3, row 4). The East region of the 3 km SingleMtn was chosen to ~~avoid the regional variation~~

295 ~~found~~isolate blocks generated in ~~NH blocking (Nakamura et al., 1997; Davini et al. 2012), however, we remind the reader that~~

296 ~~surface forcing in the SH is asymmetric (e.g. Berrisford et al. 2007). 3 km SingleMtn East blocks were chosen to subset blocks~~

297 ~~into those~~the model that form near the high-pressure anomaly of stationary waves. ~~Only the 3 km SingleMtn East results are~~

298 ~~shown because~~However, block-centered composites for ~~the different topographic~~all orographic configurations (i.e. 1 km, 2

299 km, 3 km, and TwoMtn), and ~~"Other"~~each of their respective regions yielded similar results (not shown~~)~~.), with little to no

300 regional variation – this result is discussed again below.

301 ~~-~~The onset of blocking ~~(Fig. 3 top row)~~ in the ~~aquaplanet composite~~composites (Fig. ~~3d~~3, column 1) is qualitatively

302 similar to that found in the case study (Fig. ~~2), ERAI SH (Fig. 3a),~~ 2). The Z500 anomalies all show a positive anomaly at the

303 center of the composite and ~~SingleMtn 3k East (Fig. 3g). Minor differences are observed however, such as stronger~~ negative

304 anomalies upstream ~~Z500' gradients in ERAI SH and SingleMtn 3k East, and weaker~~. In the NH, this upstream anomaly has

305 two closed centers (Fig 3a), whereas the SH and the idealized configurations each have only one. We have subset the NH

306 observations for the North Atlantic and North Pacific (not shown), and this difference is mainly due to the blocks in the North

307 Atlantic.

308 The reanalysis and idealized model results all show $\vec{W}$ convergence (i.e., blue shading) on the downstream-

309 equatorward flanks of composite blocks during onset (shading in ~~SingleMtn 3k East.~~ Fig. 3, column 1). The $\vec{W}$ convergence

310 is stronger in the SH and the aquaplanet (Figs. 3b and 3c) when compared to the NH and the idealized configurations that

311 include orography (Figs. 3a and 3d). $\vec{W}$ (vectors in Fig. 3) are weaker in the NH at onset (Fig. 3a) as compared to the SH and

312 the idealized model. This difference is mainly attributable to the blocks in the North Pacific (not shown) and is likely due to

313 the fact that the $\vec{W}$ shown are for low-frequency eddies only. As discussed in Nakamura et al. (1997), the North Pacific,

314 contributions from low-frequency eddies plays a lesser relative role as compared to the North Atlantic.

315 For composites over blocks at maximum strength (Fig. 3 middle ~~row),~~column), the positive Z500 anomaly has

316 strengthened, and a similar pattern of $\nabla \cdot \vec{W}$ is observed between the ~~3~~reanalysis and the models ~~(Figs. 3b, 3e, and 3h).~~.

317 Convergence of $\vec{W}$ on the downstream, equatorward flank of the composite blocks are enhanced compared to onset, and the

318 envelope of greatest $\vec{W}$ is now within the high-pressure center. Upstream, downstream, and equatorward low-pressure centers

319 are also evident when the composite blocks are at peak strength, though the pattern is not as clean in idealized model

320 composites (Figs. ~~3e and 3h) compared to ERAI SH (Fig. 3b). Also, the equatorward cyclone in ERAI SH (Fig 3b) is further~~

321 ~~upstream than in the idealized cases.~~3g and 3h) compared to reanalysis (Figs. 3e and 3f).

11

On the final day (bottom row, Figs 3c, 3f, and 3i of the block life cycles (Fig 3., third column), each respective composite block's Z500 anomaly weakens, and low-pressure is concentrated downstream from the block. Weak values of $\vec{W}$ exit the block downstream of the high-pressure maximum during this time (Fig. 3c, 3f, 3i). This is all consistent with downstream development (Danielson et al., 2005). A net divergence of $\vec{W}$ from the blocked region is indicative of a return to westerly zonal flow as the block dies out. The buildup of $\vec{W}$ upstream and inside the composite block during amplification, and the release of $\vec{W}$ downstream during decay is consistent with downstream development as described in Danielson et al., 2005.

The blockBlock-centered composites for the aquaplanet are qualitatively similar to composites for ERAI reanalysis, and the similarities are strongest between SH, and the idealized model configurations with mountains in terms of the evolution of Z500', $\vec{W}$, $\nabla \cdot \vec{W}$. The likeness of the and aquaplanet to ERAI SH is interesting due to the idealized conditions in the model, as well as the lack of topography. These results(Fig. 3). This is consistent with the fact that the SH has less orography than the NH. However, we remind the reader that surface forcing in the SH is still asymmetric, as discussed in Berrisford et al. (2007). Overall, however, the similarities for the model and reanalysis, regardless orography, show the potential utility of an aquaplanet model for understanding the fundamental physics of blocking. The similarities Similarities between blocks in the aquaplanet and the topographicorographic configurations show that blocks behave in a similar manner with or without mountains as a source of zonally asymmetric forcing. Having shown that individual blocking events behave as expected in the idealized

On the other hand, the differences between the NH and SH in observations are greater than the differences between the aquaplanet and the blocks in the model configured with mountains (and this result is true even if we use all blocks in the 3km single-mountain model rather than just those near the anticyclonic anomaly of the stationary wave). Thus, the model is missing some details of the internal dynamics of the blocks, as it related to the presence of orography. With this in mind, we now shift our focus to the climatological flow features and blocking climatology.

3.2 Climatological Analysis

The majority of theories on blocking formation and maintenance (summarized in the review by Woollings et al. 2018) imply that stationary waves, storm tracks, and upper level mean flow all might play important roles setting the spatial distribution of blocking frequency. These quantities are now examined for the aquaplanet, reanalysis, and model integrations with mountains. In our discussion of the climatological features in reanalysis and the SingleMtn configurations, we have chosen the following approach: we first discuss the stationary wave because it is the most fundamental metric that changes when adding mountains; then, we discuss blocking and its relationship to the jet stream. We close the analysis with a discussion of the storm tracks. This choice of the order is motivated by recent theory from Nakamura and Huang (2018) that put greater emphasis on the influence of the jet stream and stationary waves on blocking.

3.2.1 The aquaplanet

For the aquaplanet, the stationary wave, storm track, and $\overline{U250}$ are zonally symmetric (Figs. 4a and 4b). However, the blocking climatology is not zonally symmetric after 30 years (Fig. 4b). We find that it takes 250 years for the aquaplanet blocking climatology to approach zonal symmetry (Figs. 4c and 4d). However, for the models with orography, the time to reach convergence is likely not as large. We deduced this from the following analysis: we generate 20-year climatologies using randomly sampled years from our 30-year integrations and compare them. For the for the configurations with orography, the blocking climatology is spatially consistent, whereas, for the aquaplanet, each climatology has a unique spatial distribution (not shown). Therefore, we believe that 30-years of model runs provides a usable level of convergence of the spatial climatology of blocking in the integrations with mountains.

3.2.2 Reanalysis

The different orographic configurations of the northern and southern hemispheres produce distinct spatial distributions of general circulation features and atmospheric blocking (Fig. 5). Stationary wave patterns can emerge due to land-sea heating contrasts, drag, and flow deflection by topography (e.g. Held et al., 2002). The two strongest regions of anomalous high-pressure in the NH are located on the windward side of the Rocky Mountains, and near the western edge of Europe (Fig. 5a). In the SH, the high-pressure maximum is southwest of South America, and a secondary maximum can be found southeast of Australia (Fig 5b). These results are consistent with previous work (Valdes and Hoskins, 1991; Quintanar and Mechoso, 1995; Held et al., 2002; White et al., 2017).

Near the high-pressure stationary wave maxima (Figs. 5a-b), regions of suppressed $\overline{U250}$ are apparent (Figs. 5c-d). These regions have been shown to be regions of local maxima for Rossby wave breaking (Abatzoglou and Magnusdottir, 2006; Bowley et al. 2018). These regions are also where blocks are found to occur most often (Figs. 5c-d), in agreement with previous work (Wallace et al., 1988; Barriopedro et al., 2006; Dunn-Sigouin, 2013; Brunner and Steiner, 2017). According to Nakamura and Huang (2018), strong positive stationary wave anomalies, and weak mean westerlies are conducive to blocking. These conditions act to slow down the "speed limit" on $\vec{W}$, leading to "traffic jams" manifested as blocking episodes. Conversely, regions of strong westerlies, and negative stationary wave anomalies have an opposite effect, hence the suppression of blocking in regions of maximal $\overline{U250}$ (Figs. 5c-d) near climatological lows (Figs. 5a-b).

Focusing next on storm tracks, we see that the entrance of the storm tracks occurs on the northeast edge of the $\overline{U250}$ maxima (Fig. 5a, 5c). The details for this relationship are discussed in Chang et al. (2002) and explored in detail for the ~~N.~~ North Atlantic in Brayshaw et al. (2009). In the SH, there are also two local maxima in the storm tracks, and they occur to the southeast of the respective $\overline{U250}$ maxima. At the storm track exit region, transient eddies play an important role in the onset (Colucci 1985) and maintenance of blocks (Shutts, 1983; Nakamura et al. 1997; Yamazaki and Itoh 2013; Pfahl et al. 2015; Wang and Kuang, 2019). This region is also where the stationary wave and blocking maxima occur (Fig. 5). There is one

386 exception in the SH however: the SH storm track exit at the eastern terminus of the Indian Ocean (i.e., 90˚ E) does not coincide

387 with a maxima in blocking or the stationary wave – but it is a region of locally weak $\overline{U250}$.

388   For the NH (SH) in this dataset, 485 (336) blocking events are found yielding a hemispherically-averaged blocking

389 frequency of 2.7 % (1.6 %). We find the differences in hemispherically averaged blocking frequency between the hemispheres

390 to be statistically significant. The greater amount of blocking in the NH is typically assumed to be a result of the relative

391 abundance of topographic features. Therefore, we will use configurations of the model to explore the effects of mountains on

392 the spatial distribution and hemispherically averaged statistics of blocking frequency.

393

3.2.3 Orographic Configurations: Single Mountain of varying height

395   Here, a single mountain is added to the aquaplanet to study the response of the idealized model blocking climatology

396 to the presence of orography. Figure 6 shows the stationary waves, storm tracks, blocking climatologies, and $\overline{U250}$ in the

397 SingleMtn integrations. In each integration, a stationary wave is induced (Figs. 6a-6d) with a high-pressure anomaly generated

398 near the coastline on the windward side of the mountain, and a low-pressure anomaly on the leeward side (Fig. 6a-d). This

399 results in a meridionally tilted stationary wave pattern that extends into the subtropics leeward of the mountain. This pattern

400 has been explained in previous idealized modeling work (Grose and Hoskins, 1979; Cook and Held, 1992; Lutsko 2016). The

401 intensity and zonal extent of the stationary wave extrema increases with mountain height (Figs. 6a-d).

402   In the SingleMtn integrations, as the height of the mountain is increased, the local maximum in the $\overline{U250}$ increases

403 as well (right column, Fig 6). This relationship between the strength of the local jet maxima and mountain height follows from

404 the thermal wind relationship and the increased temperature gradient in the lower troposphere downstream of the mountain.

405 This mechanism is also apparent in Brayshaw et al. (2009). The stronger temperature gradient is due to enhanced cold

406 advection in the runs with taller mountains. This pattern of the $\overline{U250}$ maximum occurring just downstream of mountains is

407 the same as what occurs for the NH in observations (Fig. 5a). Across models, localized strengthening near the maximum $\overline{U250}$

408 is accompanied by a weakening of $\overline{U250}$ further downstream. In regions poleward of the midlatitude minimum in $\overline{U250}$,

409 blocking is most abundant (Figs. 6e-h). This region also coincides with the high-pressure maximum of the stationary wave

410 (Figs. 6a-d). The weakened flow and positive stationary wave anomaly here are consistent with a region of lowered $\vec{W}$ "speed

411 limit" (Nakamura and Huang, 2018), and thus enhanced block frequency. Figures 6e-h shows that these regions have

412 significantly more blocking compared to the extended aquaplanet run. On the other side of the mountain, block frequency is

413 significantly suppressed near the low-pressure stationary wave anomaly, poleward of the $\overline{U250}$ maximum.

414   The presence of mountains also leads to localized storm track maximum in each of the SingleMtn configurations

415 (Figs. 6a-d). The storm track maximum straddles the stationary wave minimum immediately downstream of the region where

416 the $\overline{U250}$ maximum also occurs (Fig. 6e-h). The storm track exit region in the idealized model does not coincide with the

417 high-pressure stationary anomaly, as it does in the NH of Earth. This allows one to work toward decoupling the response of

418   blocking to each feature. The main blocking maximum occurs near the stationary wave maximum, which is 60° longitude east

419   of the storm track exits. Near the storm track exit region, where the stationary waves are near neutral (i.e. near 90 W), there

420   are suggestions of secondary blocking maxima (Fig. 6e-h). This region is perhaps related to the breaking of Rossby waves at

421   the end of the storm track and a local block genesis region associated with strong extratropical cyclones. This would be

422   consistent with theories linking blocking to Rossby wave-breaking (Pelly and Hoskins, 2003; Berrisford et al., 2007; Masato

423   et al. 2012).

424   The zonal extent of the blocking climatology maximum increases when mountain height is increased (Figs. 6e-h).

425   This agrees with the response of the stationary wave (Figs. 6a-d). The overall hemispherically averaged statistics of blocking

426   frequency yields an increase in blocking when mountain height is increased (See Table 2). These increases for the 2k-4k

427   configurations are modest however and should be taken with some degree of caution. Still, it is clear that as mountain height

428   increases, there is a greater area of significantly more blocking compared to the aquaplanet (Figs. 6e-h). Also worth noting is

429   hemispherically-averaged blocking frequency is significantly greater in the 2k, 3k, and 4k mountain runs when compared with

430   aquaplanet. Next, we investigate the response of adding an additional mountain.

431

432   **3.2.4 Topographic Configurations: 2 Mountains**

433   For this analysis, two 3 km-high Gaussian mountains centered at 45° N with 120° of longitude between them are

434   added to the aquaplanet. The placement of the mountains is meant to create a wide and short ocean basin, as observed in the

435   NH of earth. 3 km height is meant to be semi-realistic; the values are lower than the maxima for the Rockies and the

436   ~~Himalayas~~Tibetan Plateau (~4400 m and ~8800 m, respectively) – however, the mountains are substantial enough to ~~have~~

437   generate obvious changes in the circulation (as evidenced in the Single Mountain experiments).

438   The addition of a second mountain induces a second trough and ridge in the stationary wave, and a second maxima

439   for the blocking climatology, storm track, and $\overline{U250}$ (Fig. 7). The intensity and zonal extent of these features, however, varies

440   with respect to each mountain and is a result of interference between the forcing (Manabe and Terpstra, 1974; Held et al.,

441   2002; White et al., 2017).

442   The TwoMtn configuration has a greater hemispherically- averaged blocking frequency than the other configurations

443   (Table 2~~.~~) and is also significantly greater than the aquaplanet. This is despite the TwoMtn configuration having a lower total

444   number of blocks than the 3 and 4 km SingleMtn configurations, respectively – meaning the blocks have a longer average

445   duration in the 2-mountain configuration (Table 3). Each mountain also creates regions of enhanced and suppressed blocking

446   frequency (Fig. 7b). However, just like the general circulation features, there are differences in the blocking climatology for

447   the two ocean basins.

448   Next, we examine the blocking climatology within each of the two ocean basins in the TwoMtn simulation (Wide

449   Basin and Short Basin, respectively, see Fig. 1 and Table 1). In the Wide Basin, there is close to a basinwide enhancement of

450   blocking frequency when compared to the single mountain cases (Figs. 6e-h, and 7b). Consistent with this enhancement, the

overall midlatitude $\overline{U250}$ climatology is much weaker in the wide basin compared to the other ocean basin and SingleMtn integrations. In the Short Basin, a separate blocking maximum exists near the high-pressure stationary wave anomaly. This maximum, albeit much weaker than its wide basin counterpart, is still significantly more than what occurs in the same region for the aquaplanet.

The proximity of the storm track maximum in the short basin makes there more likely to be times in which storm development occurs just upstream of the mountain; this coupled with a strong background westerly flow would inhibit blocking and perhaps explains the discrepancies between the wide basin and short basin maxima. The shorter ocean basin containing much less blocking is not consistent with what is observed in the NH of Earth, where the Atlantic has a slightly stronger blocking maximum. It seems more elaborate landmasses than this simplified case are needed to better simulate what is observed between the Atlantic and Pacific blocking climatologies in the NH.

3.3 Block Duration Statistics

One of the characteristics that allows blocks to influence midlatitude weather is their persistence. As such, we examine the influence of mountains on block persistence using our duration metric. First, we find that adding mountains leads to at least a modest increase in the average midlatitude block duration (Table 3). All topographic configurations aside from 1 km SingleMtn, also have 7-39 more blocks than the aquaplanet (Table 3). This helps to explain some of the climatological differences in block frequency between the idealized model configurations (Table 2), particularly for the 1 km SingleMtn case. Despite a 0.25 day greater mean block duration (Table 3), 1 km was found to have less hemispherically averaged blocking than the aquaplanet (Table 2) due to 21 less events. The blocks in the topographic integrations were then put into subsets based off those originating near the high-pressure stationary wave anomaly and those that were not.

Regions used to subset blocks are denoted as "East", those originating at the eastern end of the ocean basin near the high-pressure stationary anomaly, and "Other", those originating elsewhere in the midlatitudes (Fig. 1a and Table 1). Figure 8 shows the probability density ~~functions~~distributions for the aquaplanet and ~~SingleMtn~~ East blocks~~.~~ from each configuration. With the exception of the 4 km run, the "East" regions of the single mountain integrations have relatively less shorter duration blocks (i.e. 5-11 days), and relatively more longer duration blocks (11 days or more) compared to the aquaplanet (Fig. 8). Blocks from the "East" regions last longer on average than aquaplanet blocks (Table 3), but the 3 km and 4 km enhancement of block duration are not significant to the 95th percentile. Mean block duration is greater for the "East" region compared to the "Other" in the single mountain configurations (Table 3), with significant differences found in the 1 km and 2 km integrations. This leads to a cautious suggestion that blocks that originate near mountains last longer on average than those that do not~~, though~~. However, the modest differences found in the 3 km and 4 km integrations must be considered~~.~~, and the nonlinear response of block duration to linear changes in topography attests the systems own internal variability.

The response of the TwoMtn configuration is much less straightforward. This integration is divided into 3 regions, Wide Basin East, Wide Basin Other, and Short Basin (Fig. 1b and Table 1); Note the Short Basin does not have distinct "East" and "Other" regions because of its shortened zonal extent. Average block duration in the "Other" region in the Wide Basin is

16

485 slightly longer than the "East", but both regions are significantly greater than the Short Basin. This coupled with more Wide

486 Basin East events (Table 3) is consistent with the weaker maximum in the blocking climatology for the Short Basin (Figure

487 7b). Perhaps this is related to the inhibition of blocking by the nearby storm track and $\overline{U250}$ maximum in the Short Basin, but

488 we do not seek to attribute a causal relationship here.

489   Our results suggest that blocks starting near mountains last longer on average than those that do not (Table 3). In

490 reality we see a similar situation where the NH has more orographic forcing compared to the SH, and also a longer average

491 block duration (8.0 days for the NH and 6.9 days for the SH). In the idealized model, the compositing analysis for the

492 aquaplanet shows similar forcing patterns by low frequency eddies ($\nabla \cdot \vec{W}$) when compared to the SingleMtn East blocks

493 (Figs. 3d-i), despite having a shorter average block duration. Perhaps these duration differences can be accounted for by

494 considering block maintenance by high frequency transients (Shutts, 1983; Nakamura et al., 1997; TN01; Yamazaki and Itoh,

495 2013; Wang and Kuang, 2019). High frequency eddy forcing has yet to be investigated in these experiments, but this will be

496 a topic of future work.

497

498 **4. Discussion**

499   To add some perspective on the role of mountains as compared to land masses with no orographic features, we analyze

500 the response of an idealized model configuration with a single flat land mass, herein referred to as 0 km (Fig. 9). The results

501 of 0 km are briefly mentioned here to primarily serve as a benchmark for this setup. This configuration is like the others that

502 include mountains in that it imposes zonally asymmetric forcing in land-sea contrast ~~and orographic drag (Pithan et al., 2016);~~:

503 The difference, however, is that that the flat land does not act a direct barrier that deflects the flow as the mountains do,

504 generating a unique stationary wave response (e.g. Held et al. 2002) (Figs 6a-d, 7a, and 9).

505   The response of $\overline{U250}$ and the storm track (Fig. 9) in 0 km agree with results by Brayshaw et al. (2009). Compared

506 to the single mountain runs, the stationary wave pattern is shifted upstream in 0 km (Figs. 6 and 9). The blocking climatology

507 maximizes (minimizes) poleward of regions where the midlatitude $\overline{U250}$ minimizes (maximizes) (Fig. 9b). In the single

508 mountain integrations, the maximum in the blocking climatology is nearly co-located with the maximum in the stationary

509 wave; For the 0 km integration, it is not. The high-pressure stationary anomaly seemingly plays less of a role in the flat case.

510 The 0 km integration has a 3.42 % hemispherically averaged block frequency, which is greater than the aquaplanet and 1 km

511 configurations but less than the others with taller mountains (Table 2).

512

513 **5. Summary and conclusions**

514   This work utilizes an idealized moist GCM to better understand atmospheric blocking. We start with an analysis of

515 blocking in an aquaplanet, then systematically add mountains to investigate the influence of orography on blocking frequency

516 and duration. As a reminder, this work focuses on four main research questions:

517   Using 1. Are blocks in an aquaplanet dynamically similar to blocks in orographically forced simulations and

518   reanalysis?

519   2.   Does the presence of orography affect the hemispherically-averaged frequency of blocking?

520   3.   How does orography affect the spatial distribution of blocking frequency?

521   4.   Does orography affect the duration of blocking events?

522   With regards to question 1, using the aquaplanet we confirm that blocks can be generated purely through eddy-eddy

523   interactions, without any zonally asymmetric forcing from the surface., consistent with onset governed by eddy-eddy

524   interactions. This result substantiates the results of Hu et al. (2008), Hassanzadeh et al. (2014), and Nabizadeh et al. (2019).

525   To expand on the results of those previous studies, we examined the dynamical life cycle of the blocks in the aquaplanet. Block

526   centered composites of $Z500'$ $Z500'$ and $\vec{W}$ show that block lifecycles in the aquaplanet include:

527   (1) Large-scale Rossby wave features with $\vec{W}$ entering the block and converging on the upstream downstream-

528   equatorward flank during onset

529   (2) Stronger $-\vec{W}$ convergence and greater concentrations of $\vec{W}$ inside the block during peak strength

530   (3) A net divergence of $\vec{W}$ emitted downstream of the block into low-pressure regions during decay

531   Similar behaviour behavior is shown for reanalysis and the idealized model configurations that include orography, affirming

532   the usefulness of a simple idealized aquaplanet model in better understanding blocks observed in reality.

533   In With regards to questions 2, 3, and 4, in experiments with orographic forcing, we modified the aquaplanet model

534   in the following ways: (1) adding a single mountain of different heights in separate integrations; and, (2) in another integration,

535   adding two 3-km high mountains placed in a manner that creates one wide and one short ocean basin. The addition of mountains

536   to the idealized model led to several changes in blocking when compared to the aquaplanet integration:

537   -   There are localized maxima in blocking, upstream of mountains; near the high-pressure maximum of the stationary

538   waves; poleward and near climatological minima in $\overline{U250}$.

539   -   There are localized minima in blocking, downstream of mountains; near the low-pressure anomaly of the stationary

540   wave; poleward and near climatological maxima in $\overline{U250}$.

541   -   There is a significant increase in hemispherically averaged blocking frequency in integrations with mountains of

542   height 2 km and greater.

543   -   There is an increase in block duration for blocks originating near mountains, though the statistics are not robust.

544   Based on ERA-Interim reanalysis, these results mirror what is observed for the NH and SH, where the NH contains more

545   topography and blocking. In the idealized model, the enhancement of block frequency near the stationary wave maximum and

546     $\overline{U250}$ minimum is consistent with these regions being conducive to the convergence (or "traffic jamming") of wave activity

547   fluxes. These regions are found to be far from the storm track exit however, which is dissimilar to the NH in reanalysis. At the

548   storm track exit region in the North Atlantic, previous work has shown that extratropical cyclones can seed blocks (Colucci

1985) or maintain them, Pfahl et al. (2015). However, in those studies the storm track exit coincides, or sits spatially close to the stationary wave maxima. In our single mountain experiments, the storm track exit is far from the stationary wave maxima, and the result is that the blocks preferentially occur at the stationary wave maxima region. This suggests that the role of the cyclones in nature may be secondary to the role of the large-scale flow. That being said, secondary blocking maxima are found near the storm track exit in the idealized model, suggesting that this location also plays a key role in anchoring where blocks most frequently occur.

We note that the influence of mountains in our model is not identical to the differences between the NH and SH in observations. First, from the block-centered composites (Fig. 3), it was clear that the NH vs SH differences in observations for Z500 anomalies and wave activity flux are larger than those found for the aquaplanet as compared to the idealized configurations with orography. This is true for the case shown in Fig. 3 (3 km single mountain) and all other model configurations with orography. Additionally, the hemispherically-averaged blocking frequency in the NH is much larger than the SH as compared to the aquaplanet versus any model configuration with mountains. On the other hand, the spatial distribution of blocking minimizes at the storm track entrance and maximizes near the anticyclonic peak of the stationary wave, is exactly captured in our model. Thus, there are some similarities for our aquaplanet and orographic configurations inconsistent with reanalysis – which may be due to deficiencies in the model (discussed below), but there are also important differences when orography is added.

Differences in blocking between the idealized model integrations accentuate the primary role of the stationary wave in determining the preferred location of blocking. Furthermore, the fact that the compositing did not show the same differences for aquaplanet vs. mountains cases as SH vs. NH implies that the subtleties of the block-centered compositing dynamics do not determine the spatial distribution of the blocks. At the same time, secondary blocking maxima at the storm track exits in the single mountain integrations suggest that synoptic forcing indeed plays an important role in blocking, consistent with the findings of previous work (Colucci 1985, Nakamura et al. 1997, Yamazaki and Itoh 2013, Pfahl et al. 2015).

One important caveat to these experiments is that land does not include orographic drag. Pithan et al. 2016 showed that orographic drag plays a key role in the tilting of the North Atlantic storm track and the frequency of European blocking episodes. The absence of drag in these experiments could be a reason for the relatively modest changes in hemispherically averaged blocking statistics, as well as the lack of regional variation in blocking within the idealized model. Furthermore, especially for the TwoMtn experiment, one must keep in mind the highly idealized nature of the orography, which does not contain Greenland nor elongated Eurasian and North American continents. Other differences (i.e. treatment of ocean, etc.) could also play a role in discrepancies in blocking between the idealized and reanalysis models, and more systematic investigation is needed.

Overall, this work elucidates fundamental information on the formation, dynamical evolution, spatial distribution, and duration of atmospheric blocking – both in an aquaplanet and configurations with zonally asymmetric forcing. One limitation in the two-mountain experiment, is that each mountain simultaneously affects the stationary wave, jet, and storm track, making it difficult to tell the order of influence each has on the blocking climatology. Understanding the interplay and

583   individual effects of these flow features is key to predicting the behavior of blocks in future climates. ~~This~~, which is a topic of

584   future work.

585

598

599 **References**

600 Abatzoglou, J. T., and Magnusdottir, G.: Planetary Wave Breaking and Nonlinear Reflection,
601   J. Climate, 19, 6139-6152, doi:10.1175/JCLI3968.1, 2006.

602 Barnes, E., Slingo, J., and Woollings, T.: A methodology for the comparison of blocking climatologies across indices, models
603   and climate scenarios. Clim. Dynam., 38, 2467-2481, doi:10.1007/s00382-011-1243-6, 2012.

604 Barriopedro, D., GarcÍa-Herrera, R., Lupo, A. R., and Hernández, E.: A Climatology of Northern Hemisphere Blocking. J.
605   Climate, 19, 1042-1063, doi:10.1175/JCLI3678.1, 2006.

606 Barriopedro, D., García-Herrera, R., and Trigo, R.: Application of blocking diagnosis methods to General Circulation Models.
607   Part I: a novel detection scheme. Clim. Dynam., 35, 1373-1391, doi:10.1007/s00382-010-0767-5, 2010.

608 Berggren, R., Bolin, B., and Rossby, C.-G.: An Aerological Study of Zonal Motion, its Perturbations and Break-down. Tellus,
609   1, 14-37, doi:10.3402/tellusa.v1i2.8501, 1949.

610 Berrisford, P., Hoskins, B. J., and Tyrlis, E.: Blocking and Rossby Wave Breaking on the Dynamical Tropopause in the
611   Southern Hemisphere. J. Atmos. Sci., 64, 2881-2898, doi:10.1175/JAS3984.1, 2007.

612 Booth, J. F., Dunn-Sigouin, E., and Pfahl, S.: The Relationship Between Extratropical Cyclone Steering and Blocking Along
613   the North American East Coast. Geophys Res. Lett., 44, 11-11,984, doi:10.1002/2017GL075941, 2017.

614 Booth J. F., Kwon, Y.-K., Ko, S., Small, J., Madsek, R.: Spatial Patterns and Intensity of the Surface Storm Tracks in CMIP5
615   Models. Journal of Climate, 30, 4965–4981. 2017.

616 Bowley, K. A., Gyakum J. R., and Atallah E. H.: A New Perspective toward Cataloging Northern Hemisphere Rossby Wave
617   Breaking on the Dynamic Tropopause. Mon. Weather Rev., 147, 409-431, doi:10.1175/MWR-D-18-0131.1, 2019

618 Brayshaw, D. J., Hoskins, B., and Blackburn, M.: The Basic Ingredients of the North Atlantic Storm Track. Part I: Land–Sea
619   Contrast and Orography. J. Atmos. Sci., 66, 2539-2558, doi:10.1175/2009JAS3078.1, 2009.

620 Brunner, L., Schaller, N., Anstey, J., Sillmann, J., and Steiner, A.: Dependence of Present and Future European Temperature
621   Extremes on the Location of Atmospheric Blocking. Geophys. Res. Lett., 45, 6311-6320,
622   doi:10.1029/2018GL077837, 2018.

623 Brunner, L., A. Steiner, 2017: A global perspective on atmospheric blocking using GPS radio occultation – one decade of
624   observations. Atmospheric Measurement Techniques, 10, 4727-4745, doi:10.5194/amt-10-4727-2017.

625 Cassou, C., Terray, L. and Phillips, A. S.: Tropical Atlantic Influence on European Heat Waves. J. Climate, 18, 2805-2811,
626   doi:10.1175/JCLI3506.1, 2005.

627 Charney, J. G., DeVore, J. G.: Multiple Flow Equilibria in the Atmosphere and Blocking. J. Atmos. Sci., 36, 1205-1216,
628   doi:10.1175/1520-0469(1979)036<1205:MFEITA>2.0.CO;2, 1979.

629 Clark, S. K., Ming, Y., Held, I. M., and Phillips, P. J.: The Role of the Water Vapor Feedback in the ITCZ Response to
630   Hemispherically Asymmetric Forcings. J. Climate, 31, 3659-3678, doi:10.1175/JCLI-D-17-0723.1, 2018.

631   Clark, S. K., Ming, Y., and Adames, Á. F.: Monsoon low pressure system like variability in an idealized moist model. J.
632   Climate. doi:10.1175/JCLI-D-19-0289.1, 2019.

633   Colucci, S. J.: Explosive Cyclogenesis and Large-Scale Circulation Changes: Implications for Atmospheric Blocking. J.
634   Atmos. Sci., 42, 2701-2717, doi:10.1175/1520-0469(1985)042<2701:ECALSC>2.0.CO;2, 1985.

635   Cook, K., Held, I. M.: The Stationary Response to Large-Scale Orography in a General Circulation Model and a Linear Model.
636   J. Atmos. Sci., 49, 525-539, doi:10.1175/1520-0469(1992)049<0525:TSRTLS>2.0.CO;2, 1992.

637   D'Andrea, F., Tibaldi, S., Blackburn, M., Boer, G., Déqué, M., Dix, M. R., Dugas, B., Ferranti, L., Iwasaki, T., Kitoh, A.,
638   Pope, V., Randall, D., Roeckner, E., Strauss, D., Stern, H., Van den Dool, W., and Williamson, D.: Northern
639   Hemisphere atmospheric blocking as simulated by 15 atmospheric general circulation models in the period 1979–
640   1988. Clim. Dynam., 14, 385-407, doi:10.1007/s003820050230, 1998.

641   Danielson, R. E., Gyakum, J. R., Straub D. N.: A Case Study of Downstream Baroclinic Development over the North Pacific
642   Ocean. Part II: Diagnoses of Eddy Energy and Wave Activity. Mon, Weather Rev., 134, 1549-1567,
643   doi:10.1175/MWR3173.1, 2006

644   Davini, P., Cagnazzo, C., Gualdi, S., and Navarra, A.: Bidimensional Diagnostics, Variability, and Trends of Northern
645   Hemisphere Blocking. J. Climate, 25, 6496-6509, doi:10.1175/JCLI-D-12-00032.1, 2012.

646   Dee, D. P., Uppala, S. M., Simmons, A. J., Berrisford, P., Poli, P., Kobayashi, S., Andrae, U., Balmaseda, M. A., Balsamo,
647   G., Bauer, P., Bechtold, P., Beljaars, A. C. M., Van de Berg, L., Bidlot, J., Bormann, N., Delsol, C., Dragani, R.,
648   Fuentes, M., Geer, A. J., Haimberger, L., Healy, S. B., Hersbach, H., Hólm, E. V., Isaksen, L., Kållberg, P., Köhler,
649   M., Matricardi, M., McNally, A. P., Monge-Sanz, B. M., Morcrette, J., Park, B., Peubey, C., de Rosnay, P., Tavolato,
650   C., Thépaut, J., and Vitart, F.: The ERA-Interim reanalysis: configuration and performance of the data assimilation
651   system. Q. J. Roy. Meteorol. Soc., 137, 553-597, doi:10.1002/qj.828, 2011.

652   Dole, R., Hoerling, M., Perlwitz, J., Eischeid, J., Pegion, P., Zhang, T., Quan, X., Xu, T., and Murray, D.: Was there a basis
653   for anticipating the 2010 Russian heat wave? Geophys. Res. Lett., 38, n/a, doi:10.1029/2010GL046582, 2011.

654   Dong, L., Mitra, C., Greer, S., and Burt, E.: The Dynamical Linkage of Atmospheric Blocking to Drought, Heatwave and
655   Urban Heat Island in Southeastern US: A Multi-Scale Case Study. Atmosphere, 9, 33, doi:10.3390/atmos9010033,
656   2018.

657   Dunn-Sigouin, E., Son, S.: Northern Hemisphere blocking frequency and duration in the CMIP5 models. J. Geophys. Res.-
658   Atmos. 118, 1179-1188, doi:10.1002/jgrd.50143, 2013.

659   E. K. M. Chang, Lee, S., and Swanson, K.L.: Storm Track Dynamics. J. Climate, 15, 2163-2183, doi:10.1175/1520-
660   0442(2002)015<02163:STD>2.0.CO;2, 2002.

661   Egger, J.: Dynamics of Blocking Highs. J. Atmos. Sci., 35, 1788-1801, doi:10.1175/1520-
662   0469(1978)035<1788:DOBH>2.0.CO;2, 1978.

663   Frierson, D. M. W.: The Dynamics of Idealized Convection Schemes and Their Effect on the Zonally Averaged Tropical
664   Circulation. J. Atmos. Sci., 64, 1959-1976, doi:10.1175/JAS3935.1, 2007.

665 Frierson, D. M. W., Held, I. M., and Zurita-Gotor, P.: A Gray-Radiation Aquaplanet Moist GCM. Part I: Static Stability and
666   Eddy Scale. J. Atmos. Sci., 63, 2548-2566, doi:10.1175/JAS3753.1, 2006.

667 Frierson, D. M. W., Held, I. M., and Zurita-Gotor, P.: A Gray-Radiation Aquaplanet Moist GCM. Part II: Energy Transports
668   in Altered Climates. J. Atmos. Sci., 64, 1680-1693, doi:10.1175/JAS3913.1, 2007.

669 Geen, R., Lambert, F. H. and Vallis, G. K.: Regime Change Behavior during Asian Monsoon Onset. J. Climate, 31, 3327-
670   3348, doi:10.1175/JCLI-D-17-0118.1, 2018.

671 Grose, W. L., Hoskins, B. J.: On the Influence of Orography on Large-Scale Atmospheric Flow. J. Atmos. Sci., 36, 223-234,
672   doi:10.1175/1520-0469(1979)036<0223:OTIOOO>2.0.CO;2, 1979.

673 Guo, Y., Chang, E. K. M., and Leroy, S. S.: How strong are the Southern Hemisphere storm tracks? Geophys. Res. Lett., 36,
674   L22806, doi:10.1029/2009GL040733. 2009.

675 Hassanzadeh, P., Kuang, Z., and Farrell, B. F.: Responses of midlatitude blocks and wave amplitude to changes in the
676   meridional temperature gradient in an idealized dry GCM. Geophys. Res. Lett., 41, 5223-5232,
677   doi:10.1002/2014GL060764, 2014.

678 Held, I. M., Ting, M., and Wang, H.: Northern Winter Stationary Waves. J. Climate, 15, 2125-2144, doi:10.1175/1520-
679   0442(2002)015<2125:NWSWTA>2.0.CO;2, 2002.

680 Hu, Y., Yang, D., and Yang, J.: Blocking systems over an aqua planet. Geophys. Res. Lett., 35, L19818-n/a,
681   doi:10.1029/2008GL035351, 2008.

682 Hodges, K. I., Lee, R. W., and Bengtsson, L.: A Comparison of Extratropical Cyclones in Recent Reanalyses ERA-Interim,
683   NASA MERRA, NCEP CFSR, and JRA-25. J. Climate, 24, 4888-4906, doi:10.1175/2011JCLI4097.1, 2011.

684 Luo, D.: A Barotropic Envelope Rossby Soliton Model for Block–Eddy Interaction. Part I: Effect of Topography. J. Atmos.
685   Sci., 62, 5-21, doi:10.1175/1186.1, 2005.

686 Lutsko, N. J., Held, I. M.: The Response of an Idealized Atmosphere to Orographic Forcing: Zonal versus Meridional
687   Propagation. J. Atmos. Sci., 73, 3701-3718, doi:10.1175/JAS-D-16-0021.1, 2016.

688 Croci-Maspoli, M., Schwierz, C., and Davies, H. C.: A Multifaceted Climatology of Atmospheric Blocking and Its Recent
689   Linear Trend. J. Climate, 20, 633-649, doi:10.1175/JCLI4029.1, 2007.

690 Manabe, S., Terpstra, T. B.: The Effects of Mountains on the General Circulation of the Atmosphere as Identified by Numerical
691   Experiments. J. Atmos. Sci., 31, 3-42, doi:10.1175/1520-0469(1974)031<0003:TEOMOT>2.0.CO;2, 1974.

692 Masato, G., Hoskins, B. J., and Woollings, T. J.: Wave-breaking characteristics of midlatitude blocking. Q. J. Roy. Meteorol.
693   Soc., 138, 1285-1296, doi:10.1002/qj.990, 2012.

694 Matsueda, M., Mizuta, R. and Kusunoki, S.: Future change in wintertime atmospheric blocking simulated using a 20-km-mesh
695   atmospheric global circulation model. J. Geophys. Res.-Atmos., 114, D12114-n/a, doi:10.1029/2009JD011919, 2009.

696 Mattingly, K. S., McLeod, J. T., Knox, J. A., Shepherd, J. M., and Mote, T. L.: A climatological assessment of Greenland
697   blocking conditions associated with the track of Hurricane Sandy and historical North Atlantic hurricanes.
698   International Journal of Climatology, 35, 746-760, doi:10.1002/joc.4018, 2015.

699 Nabizadeh, E., Hassanzadeh, P., Yang, D., and Barnes, E. A.: Size of the Atmospheric Blocking Events: Scaling Law and
700   Response to Climate Change. Geophys. Res. Lett., 46, 13488-13499, doi:10.1029/2019GL084863, 2019.

701 Nakamura, H., Nakamura, M., and Anderson, J. L.: The Role of High- and Low-Frequency Dynamics in Blocking Formation.
702   Mon. Weather Rev., 125, 2074-2093, doi:10.1175/1520-0493(1997)125<2074:TROHAL>2.0.CO;2, 1997.

703 Nakamura, H., Shimpo, A.: Seasonal Variations in the Southern Hemisphere Storm Tracks and Jet Streams as Revealed in a
704   Reanalysis Dataset. J. Climate, 17, 1828-1844, doi:10.1175/1520-0442(2004)017<1828:SVITSH>2.0.CO;2, 2004.

705 Nakamura, N., Huang, C. S. Y.: Atmospheric blocking as a traffic jam in the jet stream. Science, 361, 42-47,
706   doi:10.1126/science.aat0721, 2018.

707 O'Gorman, P. A., Schneider, T.: The Hydrological Cycle over a Wide Range of Climates Simulated with an Idealized GCM.
708   J. Climate, 21, 3815-3832, doi:10.1175/2007JCLI2065.1, 2008.

709 Parsons, S., Renwick, J. A., and McDonald, A. J.: An Assessment of Future Southern Hemisphere Blocking Using CMIP5
710   Projections from Four GCMs. J. Climate, 29, 7599-7611, doi:10.1175/JCLI-D-15-0754.1, 2016.

711 Pelly, J. L., Hoskins, B. J.: A New Perspective on Blocking. J. Atmos. Sci., 60, 743-755, doi:10.1175/1520-
712   0469(2003)060<0743:ANPOB>2.0.CO;2, 2003.

713 Pfahl, S., Schwierz, C., Croci-Maspoli, M., Grams, C. M., and Wernli, H.: Importance of latent heat release in ascending air
714   streams for atmospheric blocking. Nat. Geosci., 8, 610-614, doi:10.1038/ngeo2487, 2015.

715 Pfahl, S., Wernli, H.: Quantifying the relevance of atmospheric blocking for co-located temperature extremes in the Northern
716   Hemisphere on (sub-)daily time scales. Geophys. Res. Lett., 39, n/a, doi:10.1029/2012GL052261, 2012.

717 Pithan, F., Shepherd, T. G., Zappa, G., Sandu, I.: Climate model biases in jet streams, blocking and storm tracks resulting from
718   missing orographic drag. Geophys. Res. Lett., 43, 7231-7240, doi:10.1002/2016GL069551, 2016.

719 Quintanar, A. I., Mechoso, C. R.: Quasi-Stationary Waves in the Southern Hemisphere. Part I: Observational Data. J. Climate,
720   8, 2659-2672, doi:10.1175/1520-0442(1995)008<2659:QSWITS>2.0.CO;2, 1995.

721 Renwick, J. A.: Persistent Positive Anomalies in the Southern Hemisphere Circulation. Mon. Weather Rev., 133, 977-988,
722   doi:10.1175/MWR2900.1, 2005.

723 Rex, D. F.: Blocking Action in the Middle Troposphere and its Effect upon Regional Climate. Tellus, 2, 196-211,
724   doi:10.3402/tellusa.v2i3.8546, 1950.

725 Sausen, R., König, W., and Sielmann, F.: Analysis of blocking events from observations and ECHAM model simulations.
726   Tellus A, 47, 421-438, doi:10.3402/tellusa.v47i4.11526, 1995.

727 Shutts, G. J.: The propagation of eddies in diffluent jetstreams: Eddy vorticity forcing of 'blocking' flow fields. Q. J. Roy.
728   Meteorol. Soc., 109, 737-761, doi:10.1002/qj.49710946204, 1983

729 Sillmann, J., Croci-Maspoli, M., Kallache, M., and Katz, R. W.: Extreme Cold Winter Temperatures in Europe under the
730   Influence of North Atlantic Atmospheric Blocking. J. Climate, 24, 5899-5913, doi:10.1175/2011JCLI4075.1, 2011.

731 Strong, C., Magnusdottir, G.: Tropospheric Rossby Wave Breaking and the NAO/NAM. J. Atmos. Sci., 65, 2861-2876,
732   doi:10.1175/2008JAS2632.1, 2008.

733 Takaya, K., Nakamura, H.: A Formulation of a Phase-Independent Wave-Activity Flux for Stationary and Migratory
734   Quasigeostrophic Eddies on a Zonally Varying Basic Flow. J. Atmos. Sci., 58, 608-627, doi:10.1175/1520-
735   0469(2001)058<0608:AFOAPI>2.0.CO;2, 2001.

736 Trenberth, K. E.: Storm Tracks in the Southern Hemisphere. J. Atmos. Sci., 48, 2159-2178, doi:10.1175/1520-
737   0469(1991)048<2159:STITSH>2.0.CO;2, 1991.

738 Troen, I. B., Mahrt, L.: A simple model of the atmospheric boundary layer; sensitivity to surface evaporation. Bound.-Lay.
739   Meteorol., 37, 129-148, doi:10.1007/BF00122760, 1986.

740 Tung, K. K., Lindzen, R. S.: A Theory of Stationary Long Waves. Part I: A Simple Theory of Blocking. Mon. Weather Rev.,
741   107, 714-734, doi:10.1175/1520-0493(1979)107<0714:ATOSLW>2.0.CO;2, 1979.

742 Valdes, P. J., Hoskins, B. J.: Nonlinear Orographically Forced Planetary Waves. J. Atmos. Sci., 48, 2089-2106,
743   doi:10.1175/1520-0469(1991)048<2089:NOFPW>2.0.CO;2, 1991.

744 Vallis, G. K., Colyer, G., Geen, R., Gerber, E., Jucker, M., Maher, P., Paterson, A., Pietschnig, M., Penn, J., and Thomson, S.
745   I.: Isca, v1.0: a framework for the global modelling of the atmospheres of Earth and other planets at varying levels of
746   complexity. Geosci. Model Dev., 11, 843-859, doi:10.5194/gmd-11-843-2018, 2018.

747 Wallace, J. M., Lim, G., and Blackmon, M. L.: Relationship between Cyclone Tracks, Anticyclone Tracks and Baroclinic
748   Waveguides. J. Atmos. Sci., 45, 439-462, doi:10.1175/1520-0469(1988)045<0439:RBCTAT>2.0.CO;2, 1988.

749 Wang, L., Z. Kuang, Z.: Evidence against a general positive eddy feedback in atmospheric blocking. arXiv preprint
750   arXiv:1907.00999. 2019

751 White, R. H., Battisti, D. S., and Roe, G. H.: Mongolian Mountains Matter Most: Impacts of the Latitude and Height of Asian
752   Orography on Pacific Wintertime Atmospheric Circulation. J. Climate, 30, 4065-4082, doi:10.1175/JCLI-D-16-
753   0401.1, 2017.

754 Wirth, V., Riemer, M., Chang, E. K. M., and Martius, O.: Rossby Wave Packets on the Midlatitude Waveguide—A Review.
755   Mon. Weather Rev., 146, 1965-2001, doi:10.1175/MWR-D-16-0483.1, 2018.

756 Woollings, T., Barriopedro, D., Methven, J., Son, S., Martius, O., Harvey, B., Sillmann, J., Lupo, A., Seneviratne, S.: Blocking
757   and its Response to Climate Change. Curr Clim Change Rep, 4, 287-300, doi:10.1007/s40641-018-0108-z, 2018.

758 Yamazaki, A., Itoh, H.: Vortex–Vortex Interactions for the Maintenance of Blocking. Part I: The Selective Absorption
759   Mechanism and a Case Study. J. Atmos. Sci., 70, 725-742, doi:10.1175/JAS-D-11-0295.1, 2013.

760

Configuration	Region	Western Edge	Eastern Edge
Single Mountain (SingleMtn)	East	0°	90° E
	Other	90° E	0°
Two Mountains (TwoMtn)	Wide Basin East	0°	90° E
	Wide Basin Other	150° W	0°
	Short Basin	90° E	150° W

761 Table 1: Regions used for subsetting blocks in the compositing and duration analysis. Each region spans 30°- 65° N, for the longitudes
762 listed in the table.

763

Configuration	Hemispherically averaged Block Frequency (%)	Standard Deviation of Hemispherically Averaged Block Frequency ~~(%), 30° N- 90° N~~(%)	Number of Events
Aquaplanet	3.24	0.84	387
1 km single mountain	3.17	0.70	365
2 km single mountain	3.67*	1.00	400
3 km single mountain	3.74*	0.90	438
4 km single mountain	3.84*	0.79	433
Two 3 km mountains (TwoMtn)	4.01*	0.99	423

764 **Table 2: Cool season area-averaged block frequency and number of events in the idealized model integrations. Asterisks indicate**
765 **values that are significantly different from the aquaplanet.**

766

	Mean block duration (days) and number of events		
	All Midlatitude Blocks	**East blocks**	**Other blocks**
Aquaplanet	7.53 (227)	-	-
1 km mountain	7.78 (206)	8.65 (58)	7.44 (148)
2 km mountain	7.93 (234)	8.54 (75)	7.64 (159)
3 km mountain	7.55 (266)	7.91 (103)	7.31 (163)
4 km mountain	7.78 (244)	7.99 (81)	7.68 (163)
Two 3 km mountains (TwoMtn)	8.17 (238)	**Wide Basin** 8.35 (81)	8.47 (86)
		Short Basin 7.65 (68)	

Table 3: Mean block duration and number of events in parentheses for midlatitude, cool season blocks in each idealized model configuration.

770
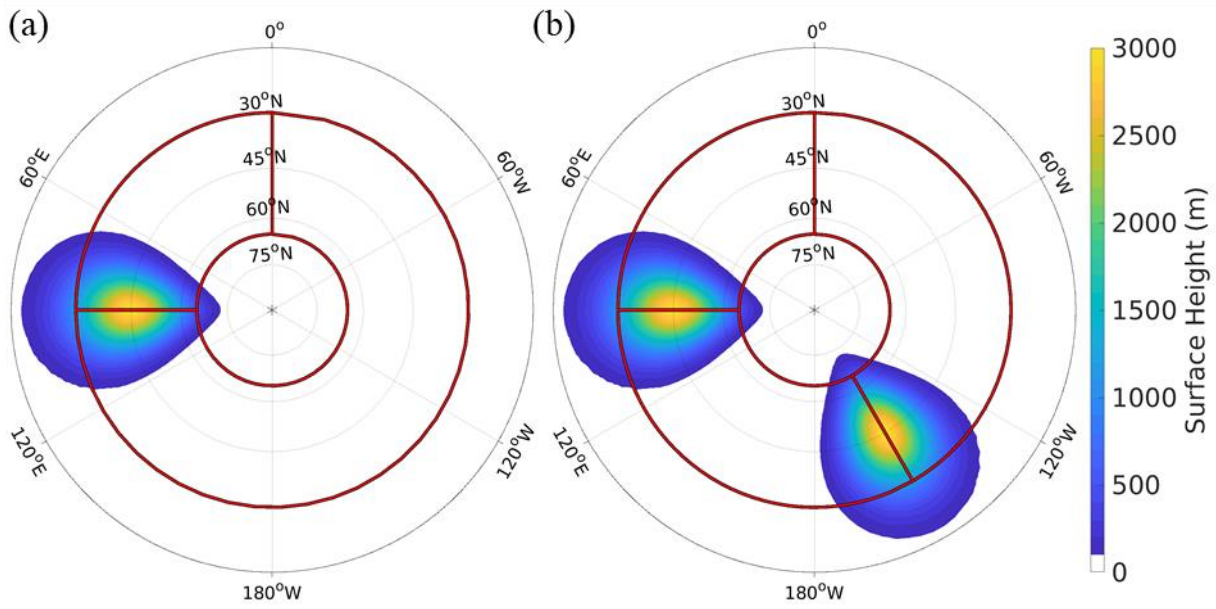
Figure 1: Surface height (shading) of the idealized model integrations with (a) a single 3 km high Gaussian mountain centered at 45
N, 90E and (b) two 3 km high Gaussian mountains centered at 45 N, 90E and 45 N, 150 W, respectively. The red outlines indicate
the block genesis regions described in Table 1.

774
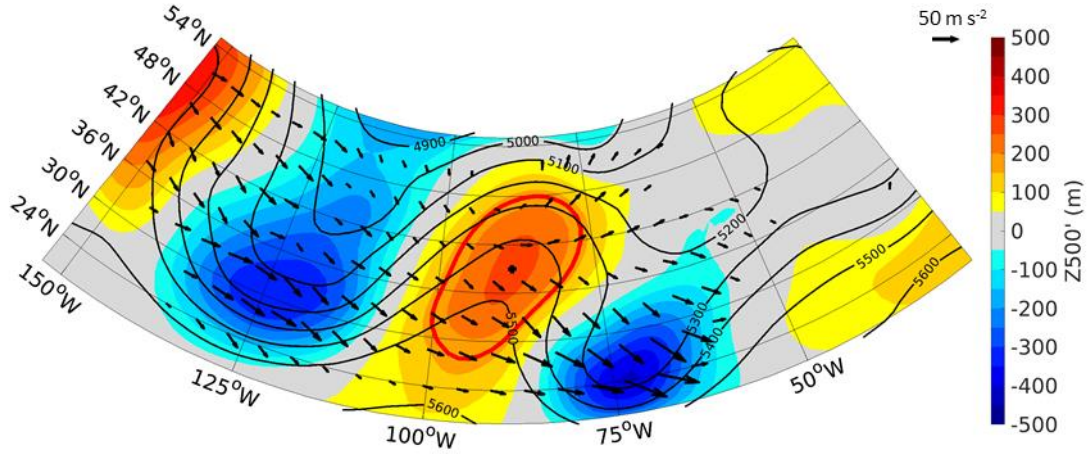
775 **Figure 2: 500 hPa geopotential height (black contours), 500 hPa geopotential height anomaly (shading), outline of blocked area (red**

776 **contour), and wave activity flux vectors $\vec{W}$ (black arrows), for the first day of a blocking episode in the aquaplanet run. The black**

777 **dot inside the block denotes the block centroid. Geopotential height contours are in 100 m intervals. $\vec{W}$ with magnitudes less than**

778 **20 m² s⁻² are removed.**

779
780

Figure 3: For cool season blocking events: Block centered composites of positive 500 hPa geopotential height anomalies (solid contours), negative 500 hPa geopotential height anomalies (dotted contours), $\vec{W}$ (arrows), and $\nabla \cdot \vec{W}$ (shading). ~~(a-c) Left~~(a, e, i) 1st Row: Computed with NH blocks over ocean in ERA-Interim. (b, f, j) 2nd Row: Computed with SH blocks in ERA-Interim. ~~(d-f) Centre~~(c, g, k) 3rd Row: Computed with blocks in the aquaplanet integration. ~~(g-i) Right~~(d, h, l) 4th Row: Computed with blocks in the 3 km single mountain integration. The ~~top~~left, middle, and ~~bottom rows~~right columns are composites over the first, strongest, and last timesteps of blocking episodes, respectively. Positive (negative) 500 hPa geopotential height anomaly contours are in 50 m (-10 m) intervals with outer contour 50 m (-30 m). $\vec{W}$ with magnitudes less than 20 m² s⁻² are removed. Latitude and longitude are defined relative to the composite block center.
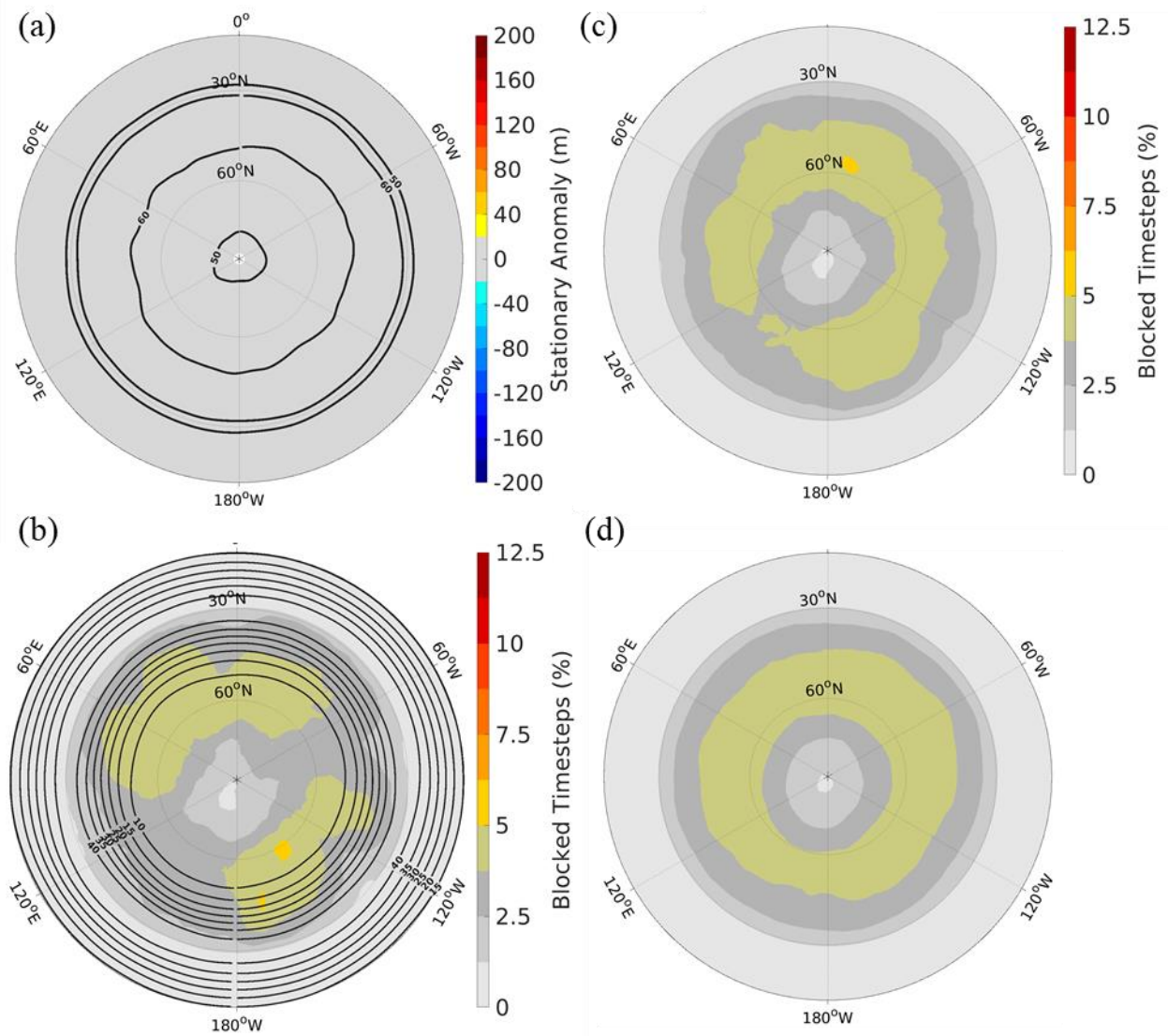
Figure 4: (a and c) Topb) Left: For 30 cool seasons (Nov.-Mar.) in the aquaplanet, (a) the stationary wave (shading) and storm track (heavy black contours), and (cb) the blocking climatology (shading) and $\overline{U250}$ (heavy black contours) for the idealized model aquaplanet integration. (bc and d) BottomRight: Blocking climatology (shading) for (c) 100 and (d) 250 cool seasons in the aquaplanet. In (a) storm track contours are in 10 m intervals where the outer contour is 50 m. In (cb) $\overline{U250}$ contours are in 5 m/s intervals where the outer contour is 30 m s^{-1}
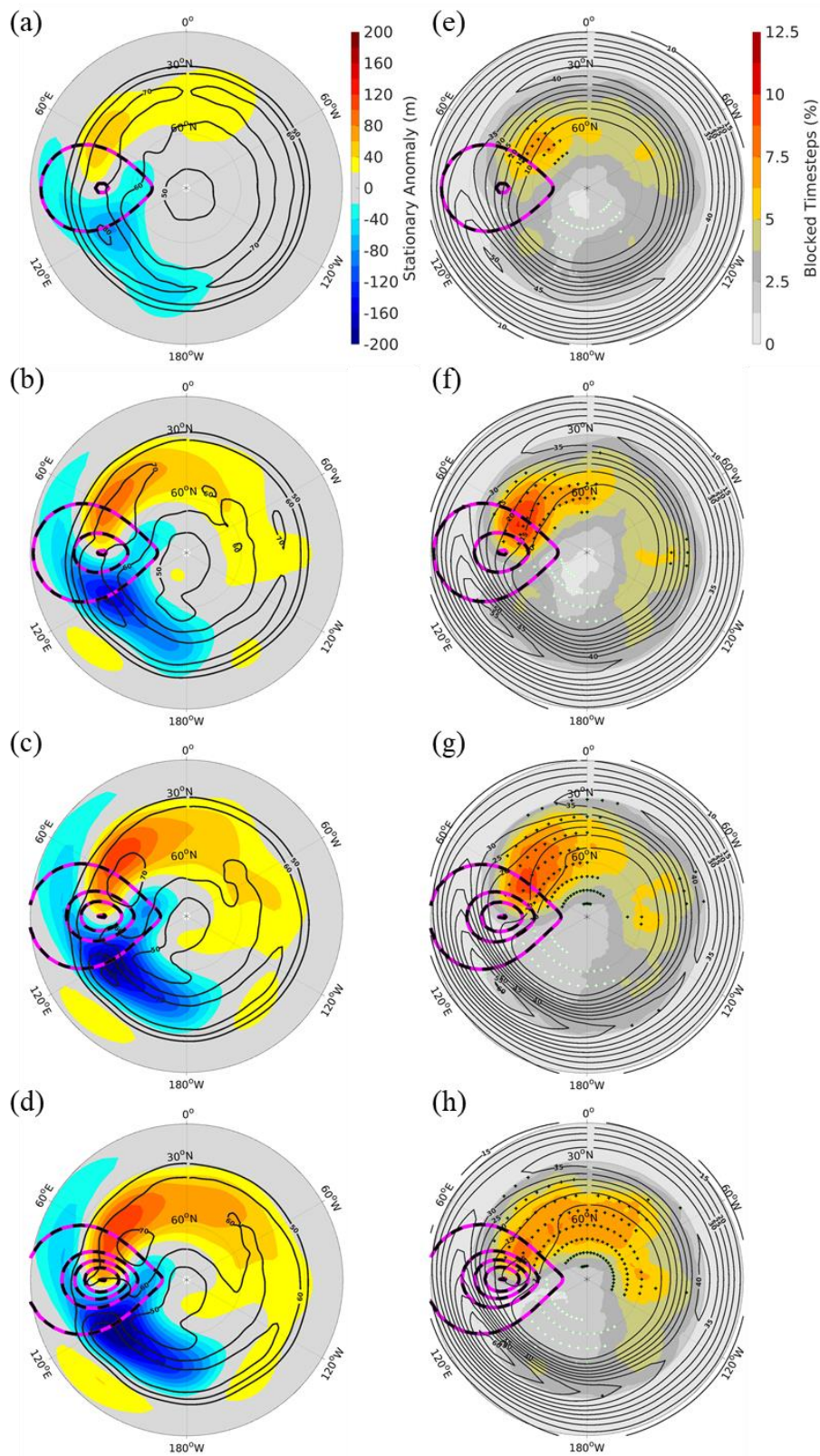
798
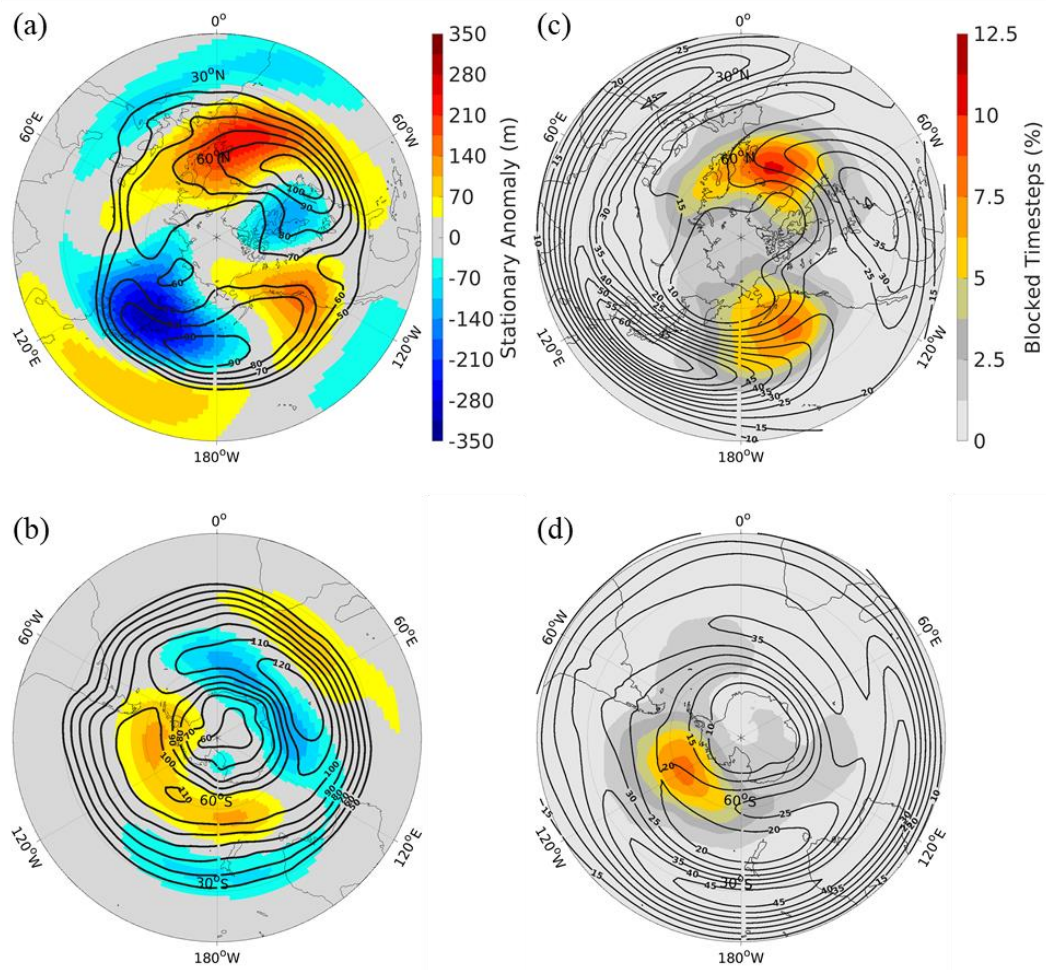
Figure 5: (a-b) Left: Cool season stationary wave (shading) and storm track (heavy black contours) for the (a) northern and (b) southern hemispheres in ERA-Interim. Storm track contours are in 10 m intervals where the outer contour is 50 m. (c-d) Right: Cool season blocking climatology (shading) and $\overline{U250}$ (heavy black contours) for the (c) northern and (d) southern hemispheres in ERA-Interim. $\overline{U250}$ contours are in 5 m/s intervals where the outer contour is 10 m s^{-1}.

803

805 Figure 6: (a-d) Left: Cool season stationary wave (shading) and storm track (heavy black contours) for the (a) 1 km, (b) 2 km, (c) 3

806 km, and (d) 4 km mountain height integrations. Storm track contours are in 10 m intervals where the outer contour is 50 m. (e-h)

807 Right: Cool season blocking climatology (shading) and $\overline{U250}$ (heavy black contours) for the (e) 1 km, (f) 2 km, (g) 3 km, and (h) 4

808 km mountain height integrations. $\overline{U250}$ contours are in 5 m/s intervals where the outer contour is 10 m s^{-1}. Black (white) stippling

809 in (e-h) indicates significantly greater (less) block frequency at nearby gridpoints when compared to a 250-year aquaplanet

810 integration. Pink and black dotted contours represent surface height, where the outer contour is the edge of the land-mask and the

811 inner contours are in 1 km intervals.

812

813
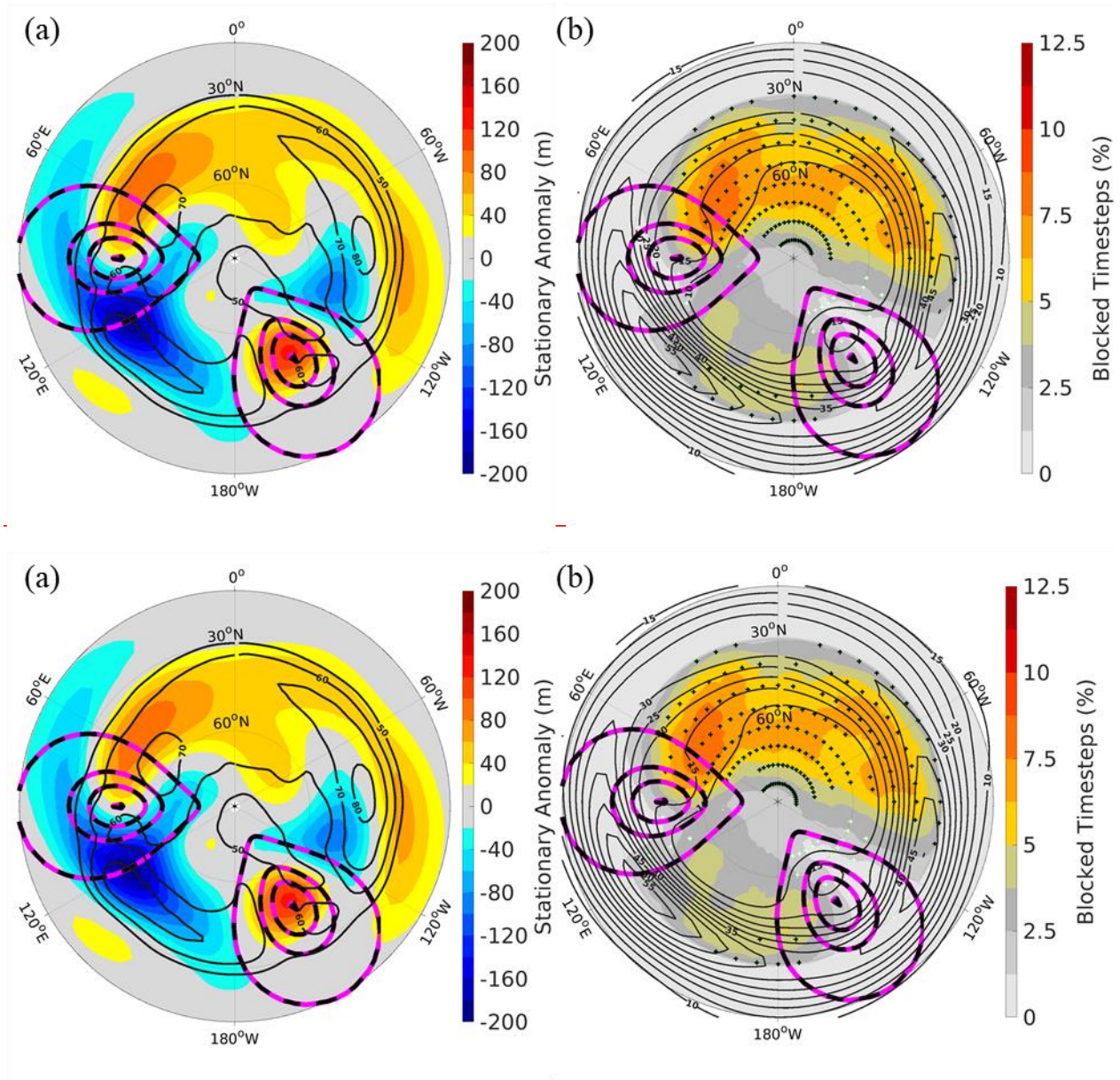
814

815 **Figure 7: For the 2-mountain idealized model integration, (a) the cool season stationary wave (shading) and storm track (heavy**

816 **black contours), and (b) the cool season blocking climatology (shading) and $\overline{U}250$ (heavy black contours). In (a) storm track contours**

817 **are in 10 m intervals where the outer contour is 50 m. In (b) $\overline{U}250$ contours are in 5 m/s intervals where the outer contour is 10 m**

818 **s^{-1}. Black (white) stippling in b indicates significantly greater (less) block frequency at nearby gridpoints when compared to a 250-**

819 **year aquaplanet integration. Pink and black dotted contours represent surface height, where the outer contour is the edge of the**

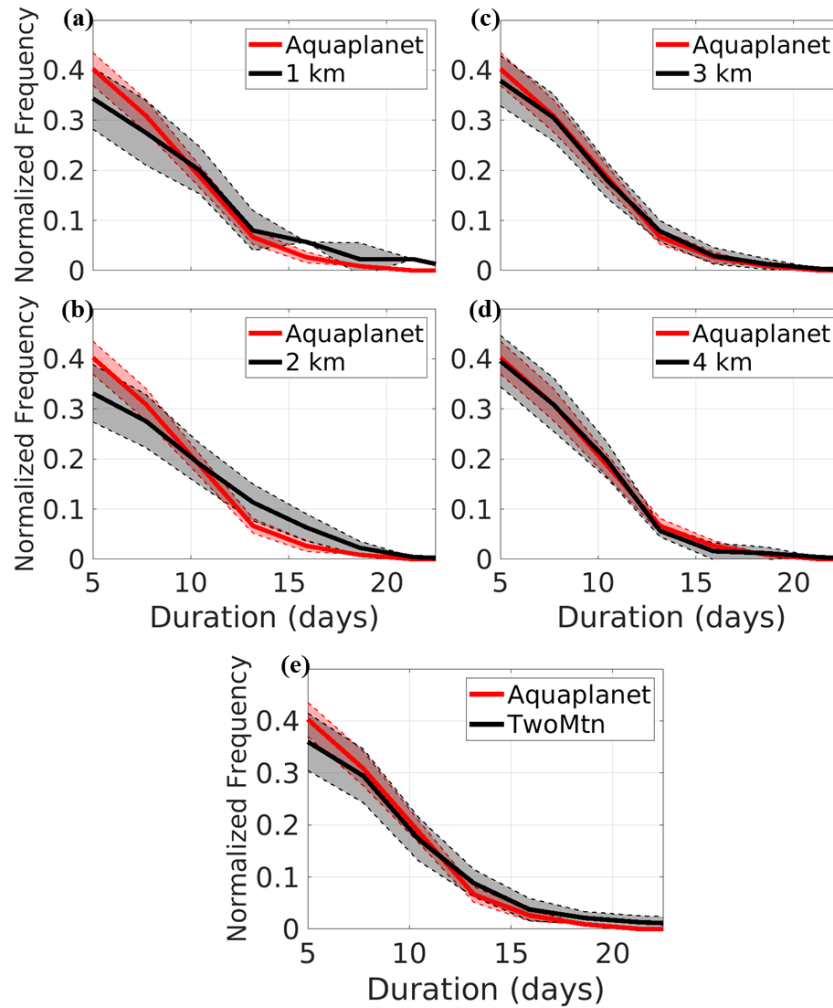820 **land-mask and the inner contours are in 1 km intervals.**

821

37

823 **Figure 8: Block duration probability density distributions for the aquaplanet and "East" blocks (as defined in table 1) in the ~~single~~**

824 **~~mountain~~ (a)SingleMtn 1 km, (b) SingleMtn 2 km, (c) SingleMtn 3 km, (d) SingleMtn 4 km, and (e) TwoMtn configurations. Thick**

825 **lines denote the mean probability density distribution for each configuration. Shaded regions bordered by dotted lines outline +/- 1**

826 **full standard deviation from the mean.**
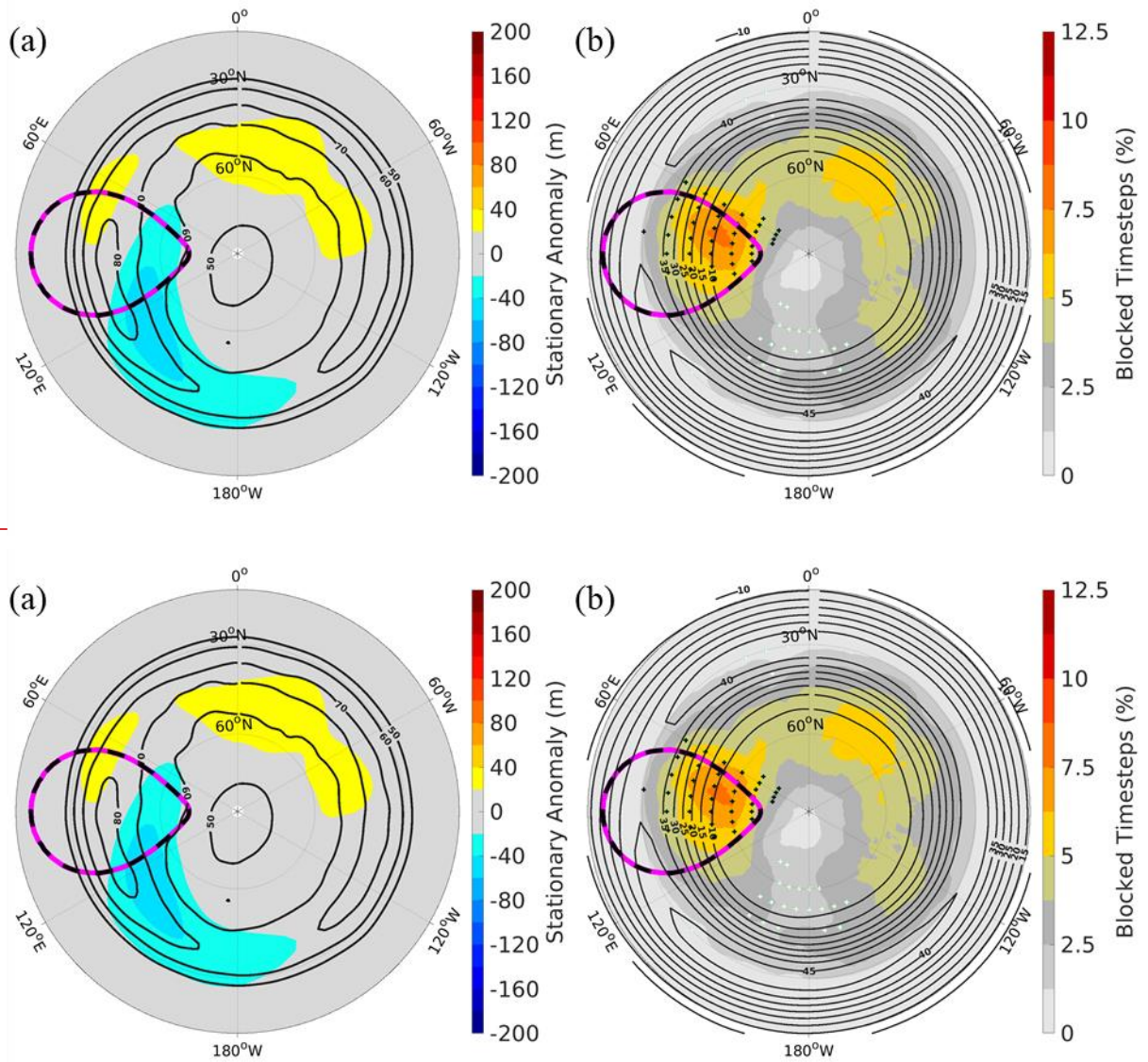
827

828

829 —

830

Figure 9: For an integration with 1 flat landmass, (a) the cool season stationary wave (shading) and storm track (heavy black contours), and (b) the cool season blocking climatology (shading) and $\overline{U250}$ (heavy black contours). In (a) storm track contours are in 10 m intervals where the outer contour is 50 m. In (b) $\overline{U250}$ contours are in 5 m/s intervals where the outer contour is 10 m s^{-1}. Black (white) stippling in b indicates significantly greater (less) block frequency at nearby gridpoints when compared to a 250-year aquaplanet integration. The pink and black dotted contours represent the outer edge of the land-mask.

39